

Ion chemistry in H₂-Ar low temperature plasmas

M. Sode, T. Schwarz-Selinger, and W. Jacob

Citation: [Journal of Applied Physics](#) **114**, 063302 (2013); doi: 10.1063/1.4817526

View online: <http://dx.doi.org/10.1063/1.4817526>

View Table of Contents: <http://aip.scitation.org/toc/jap/114/6>

Published by the [American Institute of Physics](#)


Articles you may be interested in

[Quantitative determination of mass-resolved ion densities in H₂-Ar inductively coupled radio frequency plasmas](#)

[Journal of Applied Physics](#) **113**, 093304093304 (2013); 10.1063/1.4794165

Looking for a specific
instrument?

Easy access to the latest equipment.
Shop the *Physics Today* Buyer's Guide.



**PHYSICS
TODAY**

lasers imaging
VACUUM EQUIPMENT instrumentation
software **MATERIALS**
cryogenics + MORE...

Ion chemistry in H₂-Ar low temperature plasmas

M. Sode,^{a)} T. Schwarz-Selinger, and W. Jacob

Max-Planck-Institut für Plasmaphysik, EURATOM Association, Boltzmannstraße 2, D-85748 Garching, Germany

(Received 28 May 2013; accepted 19 July 2013; published online 8 August 2013)

A rate equation model is devised to study the ion composition of inductively coupled H₂-Ar plasmas with different H₂-Ar mixing ratios. The model is applied to calculate the ion densities n_i , the wall loss probability of atomic hydrogen β_H , and the electron temperature T_e . The calculated n_i 's of Ar⁺, H⁺, H₂⁺, H₃⁺, and ArH⁺ are compared with experimental results. Calculations were made for a total gas pressure of 1.0 Pa. The production and loss channels of all ions are presented and discussed in detail. With the production and loss rates, the density dependence of each ion on the plasma parameters is explained. It is shown that the primary ions H₂⁺ and Ar⁺ which are produced by ionization of the background gas by electron collisions are effectively converted into H₃⁺ and ArH⁺. The high density of ArH⁺ and Ar⁺ is attributed to the low loss to the walls compared to hydrogen ions. It is shown that the H⁺/H₂⁺ density ratio is strongly correlated to the H/H₂ density ratio. The dissociation degree is around 1.7%. From matching the calculated to the measured atomic hydrogen density n_H , the wall loss probability of atomic hydrogen on stainless steel β_H was determined to be $\beta_H = 0.24$. The model results were compared with recently published experimental results. The calculated and experimentally obtained data are in fair agreement. [<http://dx.doi.org/10.1063/1.4817526>]

I. INTRODUCTION

In surface engineering, H₂-containing plasmas have a wide range of applications, for example, in etching,¹ film deposition^{2–7} and surface passivation, hydrogenation, and oxide reduction.^{8–11} Furthermore, H₂-Ar mixtures were successfully applied for hydrogenation of thin film transistors¹² and to control the surface properties of polymers.¹³ Hopf *et al.* observed chemical sputtering of hydrocarbon films with very high rates if energetic Ar and atomic hydrogen interact simultaneously¹⁴ with carbonaceous surfaces. Therefore, Voitsenya *et al.* proposed H₂-Ar discharges for the removal of hydrocarbon deposits in magnetic fusion devices.¹⁵

In a previous study, ion densities, the electron density, the electron temperature, the gas temperature, and the dissociation degree were measured in a H₂-Ar inductively coupled low-temperature plasma.¹⁶ Quantitative results for the considered ion species were shown as a function of Ar fraction. With the electron density measured with the Langmuir probe and a simple model for the sheath, absolute densities of all ion species present in the plasma were determined. In addition, electron temperature, atomic hydrogen density, and gas temperature were measured.

To enable a comparison of these experimental results,¹⁶ in particular, the ion densities, we devised a rate equation model. Comparable models for H₂-Ar low-temperature plasmas have been published earlier. For example, Kimura and Kasugai measured the electron temperature and electron density as well as the density of atomic hydrogen in argon hydrogen inductively coupled plasma (ICP) plasmas and compared the results with a global model of the discharge.¹⁷ They also presented modeling results for the mass-resolved ion fluxes

but unfortunately they did not measure them. Hjartarson *et al.*¹⁸ studied a global model for a low pressure high density H₂-Ar discharge. Ion densities were calculated but only compared to uncalibrated signal intensities of the ion species from Gudmundsson.^{19,20} Comparable quantitative comparisons between experimental and modeling results were previously published for hollow cathode dc discharges in H₂-Ar mixtures by Méndez and coworkers.^{21,22} Their glow discharge is operated at a high voltage of several hundred volts and the sheath is relatively thick. The ion mean free path length for their plasma conditions (between 0.5 and 10 Pa) is smaller than the sheath thickness. Therefore, collisions of high energetic ions in the sheath occur, which significantly change the ion energy and ion species distributions. Furthermore, they have to take high energetic electrons (>50 eV) into account to describe the appearance of Ar²⁺ well. The ion species Ar²⁺ was not observed experimentally in our studies due to the absence of such high energetic electrons. As a result, a direct comparison with the here studied system is not possible.

The article is organized as follows: A short description of the measured quantities is given in Sec. II. In Sec. III, the rate equation model is presented. In Sec. IV, the calculated results are presented. The discussion is given in Sec. V. The summary can be found in Sec. VI.

II. EXPERIMENT

In the following, we subsume briefly the experimental results. A detailed description of the experimental procedures as well as the measured results can be found in Ref. 16. The experimental setup consists of a cylindrical stainless steel plasma chamber. The discharge is generated by a planar coil with 5 turns and 100 mm in diameter. The

^{a)}Electronic mail: maik.sode@ipp.mpg.de

coil is driven by a radio frequency (rf) generator with a maximum power of 600 Watt operating at 13.56 MHz (Dressler Cesar 136). The coil is separated from vacuum by a quartz dome.²³ The top part of the dome is 10 mm thick and acts as the dielectric window for the rf power. The outer diameter d_{el} of the quartz dome and the upper steel electrode is $d_{el} = 2r_{el} = 131$ mm where r_{el} is the corresponding radius. The distance l_{el} between both electrodes is $l_{el} = 60$ mm. The plasma is mainly generated in the assumed cylinder with the volume $V = \pi r_{el}^2 l_{el}$ between the two electrodes. Fig. 1 shows a schematic representation of the plasma chamber.

Measurements were conducted for a total gas pressure of 1.0 Pa. The plasma chamber was pumped with a turbo molecular pump with Hohlweck stage to achieve a good compression also for H_2 . A butterfly valve in front of the turbo molecular pump allows to throttle the pumping speed. All experiments were conducted with a fixed butterfly position, so that the residence time of the species was constant. The incoming gas flows were adjusted with mass-flow controllers. Mass spectrometer investigations have shown that the flux ratios of Ar and H_2 are not identical to the partial pressure ratios for the applied experimental conditions. The actual Ar partial pressure fractions f_{Ar} used in the experiment were, therefore, determined with a mass spectrometer.¹⁶ The partial pressure fractions for Ar and H_2 for determining f_{Ar} were measured prior to plasma ignition. These values do not differ significantly from the values measured after plasma ignition.

The H_2 -Ar plasmas were characterized by an energy-dispersive mass spectrometer (plasma monitor, PM), a

retarding field analyzer, optical emission spectroscopy, and a Langmuir probe. A procedure was presented that allows determining quantitatively the absolute ion densities of Ar^+ , H^+ , H_2^+ , H_3^+ , and ArH^+ from the plasma monitor raw signals. This calibration procedure included applying a Langmuir probe to convert plasma monitor signals in absolute fluxes. The conversion from fluxes to densities was based on a sheath and density profile model. The calibration procedure resulted in a significant change of the relative contributions of the H_x^+ , Ar^+ , and ArH^+ plasma monitor signals compared with the derived absolute densities for the ArH^+ , Ar^+ , and the H_x^+ ions. This is mainly due to two factors: the mass dependence of the transmission of the PM and the conversion from ion fluxes to ion densities.

The rotational temperature, T_{rot} , of the hydrogen molecule was derived from the rotational lines $Q_1 - Q_3$ of the Q-branch of the H_2 Fulcher- α diagonal band ($v' = v'' = 2$) to (540 ± 50) K. This value was taken as an estimate of the gas temperature and was applied to calculate the gas densities for the model. The dissociation degree of hydrogen is here defined as n_H/n_{H_2} with n_H being the atomic hydrogen density and n_{H_2} the molecular hydrogen density in the plasma. n_H/n_{H_2} was determined by actinometry using the ratio of the H_β/Ar_{750} lines. The dissociation degree was around 1.7% with an error $\Delta(n_H/n_{H_2}) = 0.4\%$. It was nearly independent on Ar content in the investigated mixing ratio range.

With the Langmuir probe, the electron energy distribution function (EEDF), the electron temperature T_e , and the electron density n_e were measured. The EEDFs of the considered plasma conditions can be described by a bi-Maxwellian distribution with two distinct electron temperatures. The low energy regions of the EEDFs are characterized by a higher electron temperature than the high energy region. T_e determined from the high energy region of the EEDF was in good agreement with the T_e determined from the plasma potential. Additionally, the electron temperature was calculated by a simple model based on the particle balance for one ion species only. A Maxwellian EEDF was used to obtain the required ionization rate coefficients for the particle balance equation. The such calculated T_e agreed with the measured values obtained from the high energy part of the EEDF.¹⁶ It was concluded that the T_e determined from the plasma potential is the most reliable T_e to characterize this plasma (see Sec. IV D in Ref. 16). The measured T_e decreases from 5.2 eV for pure H_2 to 2.9 eV for pure Ar. Increasing the Ar fraction at constant rf input power caused a strong increase of the plasma density. Therefore, the rf power was adjusted in order to minimize the variation in n_e . n_e was maintained in a range of about $3 \times 10^{16} \text{ m}^{-3}$ for all Ar containing mixtures. For the pure H_2 plasma, n_e decreased to about $1 \times 10^{16} \text{ m}^{-3}$.

The measured mass-resolved ion densities n_i of species i and the electron density n_e are shown in Fig. 2 as function of f_{Ar} . The considered H_2 -Ar plasma consists of five main ion species. For the pure hydrogen plasma, the dominant ion species is the H_3^+ ion with a measured density of $6.3 \times 10^{15} \text{ m}^{-3}$. H_2^+ and H^+ show a 3 times and 20 times lower measured density than H_3^+ , respectively. With increasing f_{Ar} , the measured H_x^+ densities ($x = 1, 2, 3$) decrease nearly exponentially with decreasing H_2 fraction while the ratio between them

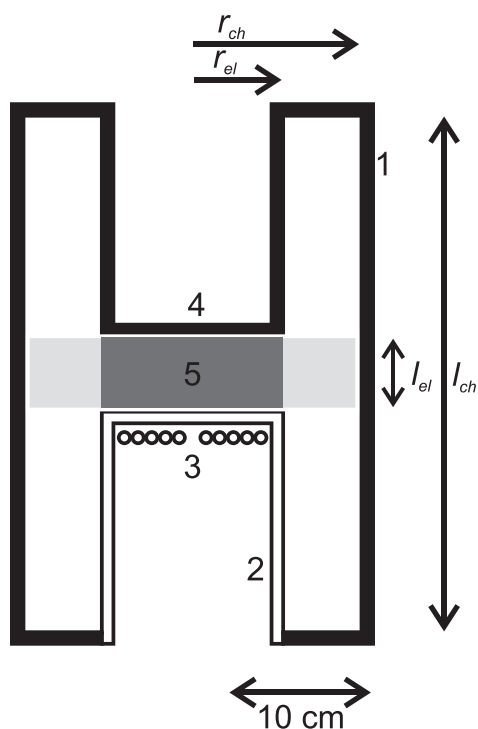


FIG. 1. Schematic representation of the plasma chamber: (1) vacuum chamber made of stainless steel, (2) quartz dome, (3) planar inductive coil, (4) upper electrode, and (5) plasma volume. The distance between the upper and lower electrode is $l_{el} = 60$ mm. The upper and lower electrodes are circular with a radius of $r_{el} = 65$ mm. The chamber has a radius of $r_{ch} = 125$ mm and the total height is $l_{ch} = 360$ mm.

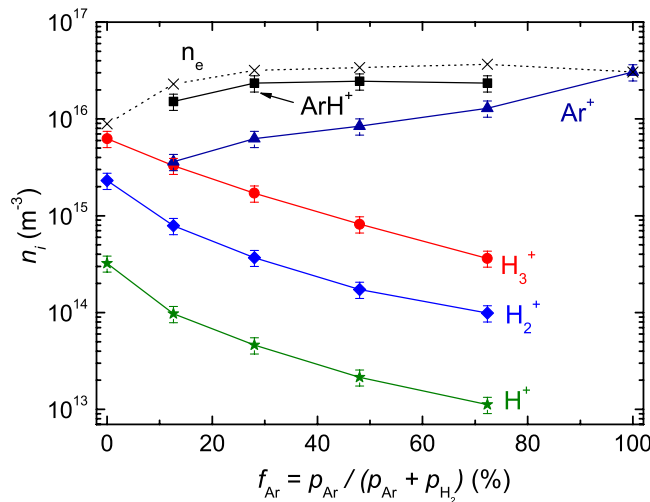


FIG. 2. Measured ion densities and electron density as a function of the Ar fraction f_{Ar} for a total pressure of 1.0 Pa.

remains roughly constant. In the mixed H_2 -Ar plasmas, the ArH^+ ion is the dominant ion and contributes about 2/3 to the total ion density in the Ar fraction range from 12.6% to 72.3%. Ar^+ is the second most abundant ion species in this range and shows as expected an increasing measured density with increasing f_{Ar} .

III. MODEL

A. General remarks

In attempts trying to theoretically describe low-temperature plasmas, typically global models are used to calculate the electron temperature, the electron density, and the species densities by solving the power and the particle balance under the quasi-neutrality condition self-consistently.^{17,18,24–26} In contrast, the model applied here considers only the particle balance under quasi-neutrality condition. As consequence, the electron density cannot be calculated in our model and has to be provided as input parameter.

We apply a rate equation system to calculate the ion densities n_i , the wall loss probability of atomic hydrogen β_{H} , and the electron temperature T_e in H_2 -Ar plasmas with different mixing ratios. The model considers six charged species (electrons, Ar^+ , ArH^+ , H^+ , H_2^+ , and H_3^+), one radical species (H atom) and the two background gas species Ar and H_2 . For argon, three excited species are considered, which are presented in Sec. III G. Altogether, the model comprises 12 species. 9 species densities are calculated. The densities of the 3 species, H_2 , Ar, and the electrons, are used as input parameters. For the particle balance, collisions in the volume and losses to the plasma-surrounding walls are taken into account. The model is zero-dimensional and predicts species densities in the plasma center. In the following subsections, the model assumptions, the calculation procedure, the volume reactions, and the wall losses are discussed in detail.

The main input parameters for the model are all the required collision rate coefficients. This data basis is explained in detail in Sec. III E. The remaining input parameters are experimentally obtained quantities, namely the

electron density n_e , the gas temperature T_g , the total pressure p , the radical density n_{H} , the Ar fraction f_{Ar} , and the geometry of the discharge vessel. The background gas densities n_j ($j = \text{H}_2$ or Ar) are calculated by the ideal gas law $n_j = p_j / (k_B T_g)$, where k_B is the Boltzmann constant. The model output values are n_i , T_e , and β_{H} . The n_i 's are obtained by solving the system of rate equations, which is explained in Sec. III C. A variation in T_e which is, strictly speaking, an input parameter in the rate equation system is used to fit the quasi neutrality as boundary condition. This is explained in detail in Sec. III D. A variation in β_{H} which is, strictly speaking, also an input parameter in the rate equation system is used to fit the calculated to the experimentally obtained atomic hydrogen density. This is explained in detail in Sec. III F 2.

B. Model assumptions

The model is based on the following assumptions and simplifications:

1. The model is 0-dimensional.
2. The loss of particles to the surrounding walls is volume averaged.
3. Electron collisions with the background gas (H_2 and Ar) are taken into account.
4. Heavy particle (i.e., ions and atomic hydrogen) collisions with the background gas (H_2 and Ar) are considered.
5. Three-body interactions are neglected due to the low pressure.
6. The temperature of the neutrals and ion species is described by one gas temperature T_g , which is set equal to the measured rotational temperature T_{rot} of the H_2 molecules. Only for atomic hydrogen, a higher temperature is used (see Sec. III F).
7. The ion and radical densities are calculated for the steady state.
8. H^- is not considered here due to very low concentrations with respect to the electron density.¹⁷
9. Vibrationally excited H_2 is not considered.
10. Excited Ar (1s and 2p states) is considered (see Sec. III G).

In general, volume recombination processes are improbable in this pressure regime and with chamber dimensions in the 100 mm range. For electron-ion recombination reactions, this is due to the low ionization degree of the order of 10^{-4} . Nevertheless, electron-ion recombination reactions are not neglected in this work but are of secondary importance. On the other hand, recombination of hydrogen atoms to molecules in the plasma volume is neglected; since for recombination, a third collision partner would be required, which is rather improbable in the considered pressure regime.

C. Particle balance

The rate equation system is based on the continuity equation

$$\frac{\partial n_i}{\partial t} + \nabla \cdot (\vec{\Gamma}_i) = R_{\text{tot}}^{iG} - R_{\text{tot}}^{iL}, \quad (1)$$

where n_i is the density of species i , $\vec{\Gamma}_i = n_i \vec{v}_i$ is the particle flux to the wall with velocity \vec{v}_i , and R_{tot}^{iG} and R_{tot}^{iL} are the total reaction rates for production (gain) and destruction (loss) of species i , respectively. In steady state, total production and loss rates must balance, so that the time variation $\partial n_i / \partial t$ for each species i is zero. In this way, a set of equations for the steady-state particle densities is compiled.

For a typical volume reaction k where a species m with density n_m reacts with species j with density n_j to create species i , the gain rate for i is

$$R_k^{iG} = n_m n_j K_k. \quad (2)$$

K_k denotes the rate coefficient for this reaction k , which is a measure for the corresponding reaction probability. Here, k is used as index for an individual reaction. Similarly, for the loss of i in a volume reaction \tilde{k} where i reacts with the species \tilde{j} , the loss frequency $\nu_{\tilde{k}}^{iL}$ is given by $\nu_{\tilde{k}}^{iL} = n_{\tilde{j}} K_{\tilde{k}}$. It is related to the corresponding reaction rate by $R_{\tilde{k}}^{iL} = n_i \nu_{\tilde{k}}^{iL}$.

D. Calculation

Solving Eq. (1), which is a rate equation system with many species, is in general associated with some difficulties briefly discussed in the following. In general, the investigated rate equation system can be nonlinear. Furthermore, the rate equations are coupled and the rate coefficients can have different powers, so that the equations become stiff. Stiffness means that the differential equation system has simultaneously solution parts, which vary very slowly in time and other parts which change very fast. To solve Eq. (1) with the aforementioned difficulties, the online available solver “Kinetic PreProcessor”^{27,28} (*KPP*) is used for the nonlinear, coupled, and stiff rate equation system. An advantage of *KPP* is that the rate equations are generated automatically from the given set of reactions. In *KPP*, the rate equation system is solved using the Rosenbrock algorithm. The algorithm is based on semi-implicit Runge-Kutta methods with adaptive stepsize. To achieve self-consistency, the quasi-neutrality has to be fulfilled which is imposed externally as an additional boundary condition. The calculated (index c) electron temperature T_e^c is varied to achieve the quasi-neutrality

$$n_e = \sum n_i, \quad (3)$$

where i is the ion species. T_e^c is accepted if the condition $0.98 \leq (\sum n_i) / n_e \leq 1.02$ is satisfied. A small change in electron temperature strongly affects the quasi-neutrality, so that the model has a high sensitivity with respect to the electron temperature. This narrow range of tolerable deviation of quasi neutrality corresponds to a variation in electron temperature of less than 1% for the considered conditions.

E. Volume collisions

The reaction rate of an arbitrary reaction k is determined by the rate coefficient K . In case of gas phase collisions, the rate coefficient is calculated by integration of $\sigma_k v_{ij}$ over the velocity distributions $f_i(\vec{v}_i)$ and $f_j(\vec{v}_j)$ of two colliding particles i and j with velocities \vec{v}_i and \vec{v}_j , respectively,

$$K_k = \langle \sigma_k v_{ij} \rangle = \int \int \sigma_k(v_{ij}) v_{ij} f_i(\vec{v}_i) f_j(\vec{v}_j) d\vec{v}_i d\vec{v}_j. \quad (4)$$

Here $v_{ij} = |\vec{v}_i - \vec{v}_j|$ is the absolute value of the relative velocity and σ_k is the cross section for the corresponding reaction. σ_k is a function of v_{ij} . Typically, σ_k is given as a function of the center-of-mass or relative energy E_{ij} where $E_{ij} = \mu_{ij} v_{ij}^2 / 2$ with the reduced mass $\mu_{ij} = m_i m_j / (m_i + m_j)$.

In this work, a Maxwellian energy distribution with temperature T_i is used to describe the particle velocity distributions. For the background gas and the ion species, this is valid because they are in thermal equilibrium. In general, for electrons, the EEDF can differ significantly from a Maxwellian EEDF. However, as outlined in Sec. II, the measured electron temperature agrees with a calculated electron temperature based on the assumption of a Maxwellian EEDF.¹⁶ Therefore, the assumption of a Maxwellian EEDF for the considered rate coefficients is reasonable.

1. Electron collisions

For collisions of electrons with heavy particles such as atoms or molecules, Eq. (4) can be rewritten because the electron mass is much lower than the atom or molecule mass and the electron energy is much higher than the heavy particle energy. The rate coefficient K_k then yields

$$K_k = \sqrt{\frac{8eT_e}{\pi m_e}} \int_0^\infty \sigma_k(E) e^{-\frac{E}{T_e}} \frac{E}{T_e} dE, \quad (5)$$

where e , m_e , E , and T_e are the elementary charge, the electron mass, the electron energy, and the electron temperature, respectively. The transformations $v_e \rightarrow E = m_e v_e^2 / (2e)$ (v_e —electron velocity), $k_B T / e \rightarrow T_e$, and $\sigma_k(v_e) \rightarrow \sigma_k(E)$ were applied to obtain an equation as a function of electron energy E because generally σ_k is given as a function of E . E and T_e are both given in eV. In the literature, the rate coefficients for electron collisions are usually given in an Arrhenius form to describe the dependence on T_e

$$K_k = K_{k0} T_e^{x_k} e^{-E_{k0}/T_e}, \quad (6)$$

where K_{k0} , x_k , and E_{k0} are constants.

The values for the considered electron collisions are compiled in Table I. From here on the reaction rates, K_k will be labeled according to the index k for the corresponding reactions, which are listed in Tables I–IV. As will be shown in Sec. IV A, ionization and dissociation of the background gas (i.e., reactions 1.1 to 1.5 in Table I) are the most important electron reactions. For these 5 reactions, K_k was calculated individually by applying Eq. (5) for a fixed T_e in steps of $\Delta T_e = 0.05$ eV. The corresponding cross sections were integrated in the energy range from the threshold energy of the considered process to at least 200 eV. The considered T_e range lies between 2 to 10 eV. In this range, the calculated K_k was fitted according to Eq. (6). σ_k were taken from Yoon *et al.*²⁹ for electron collisions with H₂, from Shah *et al.*³⁰ for electron collisions with H, and from Wetzel *et al.*³¹ for electron collisions with Ar. Yoon *et al.*²⁹ compiled a collection of

TABLE I. Reaction set with rate coefficients K for electron collisions with index k (T_e in eV). The rate coefficients of the most important reactions 1.1–1.5 are calculated from the corresponding cross sections, which are taken from the indicated references. Reactions 1.6–1.10 are of lower importance and the corresponding K 's are directly taken from the given references.

k	reaction	K (m^3s^{-1})	Reference
1.1	$\text{e}^- + \text{H}_2 \rightarrow 2\text{H} + \text{e}^-$	$8.4 \times 10^{-14} T_e^{-0.45} \times e^{-11.18/T_e}$	σ from 29
1.2	$\text{e}^- + \text{H} \rightarrow \text{H}^+ + 2\text{e}^-$	$1.1 \times 10^{-14} T_e^{0.29} \times e^{-15.28/T_e}$	σ from 30
1.3	$\text{e}^- + \text{H}_2 \rightarrow \text{H}_2^+ + 2\text{e}^-$	$2.3 \times 10^{-14} T_e^{0.19} \times e^{-17.87/T_e}$	σ from 29
1.4	$\text{e}^- + \text{H}_2 \rightarrow \text{H}^+ + \text{H} + 2\text{e}^-$	$9.4 \times 10^{-16} T_e^{0.45} \times e^{-29.94/T_e}$	σ from 29
1.5	$\text{e}^- + \text{Ar} \rightarrow \text{Ar}^+ + 2\text{e}^-$	$3.7 \times 10^{-14} T_e^{0.38} \times e^{-17.64/T_e}$	σ from 31
1.6	$\text{e}^- + \text{H}_2^+ \rightarrow \text{H}^+ + \text{H} + \text{e}^-$	$1.5 \times 10^{-13} \times e^{-1.97/T_e}$	K from 17
1.7	$\text{e}^- + \text{ArH}^+ \rightarrow \text{Ar} + \text{H}$	1.0×10^{-15}	K from 32
1.8	$\text{e}^- + \text{H}_3^+ \rightarrow 3\text{H}$	$2.8 \times 10^{-15} T_e^{0.48}$	K from 32
1.9	$\text{e}^- + \text{H}_3^+ \rightarrow \text{H}_2 + \text{H}$	$1.6 \times 10^{-15} T_e^{0.48}$	K from 32
1.10	$\text{e}^- + \text{H}_2^+ \rightarrow 2\text{H}$	$1.4 \times 10^{-15} T_e^{0.43}$	K from 32

recommended values of cross sections for electron collisions with hydrogen molecules. We consider these data as the presently most reliable data set. Shah *et al.*³⁰ and Wetzel *et al.*³¹ measured electron ionization cross sections and compared their results to existing literature data. Their values agree with published data within 15%. The remaining rate coefficients ($k = 1.6$ –1.10) were taken directly from literature. For electron-ion recombination processes (reactions 1.7 to 1.10), the rate coefficients are taken from Florescu-Mitchell and Mitchell³² where values for dissociative recombination of several molecular ions are tabulated and reviewed.

A comparison of the most important K_k 's with other literature sources was made to assess the scatter of the data. K_k with $k = 1.1$ –1.5 presented in Table I were compared to data from Hjartarson *et al.*¹⁸ and Kimura and Kasugai¹⁷ in a T_e range of 3 to 7 eV. Hjartarson *et al.* used the same literature source for $\sigma_{1.1}$ – $\sigma_{1.3}$. Probably due to different fit procedures and different considered energy and T_e ranges, the here presented $K_{1.1}$ – $K_{1.3}$ differ by up to 10% from Hjartarson *et al.* Reaction 1.4 was not considered by Hjartarson *et al.*, therefore, we cannot compare. For the ionization of Ar, Hjartarson *et al.*¹⁸ used the cross sections of Ref. 33 whereas we used Ref. 31. The difference for $K_{1.5}$ amounts to 15%. Kimura and Kasugai¹⁷ used for the hydrogen reactions cross sections of Janev *et al.*³⁴ to calculate their rate coefficients. A comparison

TABLE II. Reaction set for ion-molecule reactions k . Rate coefficients K are taken from different literature sources as indicated. *— K is calculated from the corresponding cross section.

k	reaction	K ($10^{-16} \text{m}^3\text{s}^{-1}$)			
		Ref. 35 (used)	Ref. 17	Ref. 18	Ref. 36*
2.1	$\text{H}_2^+ + \text{H}_2 \rightarrow \text{H}_3^+ + \text{H}$	20	20	20	24
2.2	$\text{ArH}^+ + \text{H}_2 \rightarrow \text{H}_3^+ + \text{Ar}$	6.3	15	15	4.5
2.3	$\text{H}_2^+ + \text{Ar} \rightarrow \text{ArH}^+ + \text{H}$	21	...	23	18
2.4	$\text{H}_2^+ + \text{Ar} \rightarrow \text{Ar}^+ + \text{H}_2$	2.0	...	2.2	3.3
2.5	$\text{H}_3^+ + \text{Ar} \rightarrow \text{ArH}^+ + \text{H}_2$	3.7	...	0.1	0
2.6	$\text{Ar}^+ + \text{H}_2 \rightarrow \text{ArH}^+ + \text{H}$	8.7	6.0	7.4	9.4
2.7	$\text{Ar}^+ + \text{H}_2 \rightarrow \text{H}_2^+ + \text{Ar}$	0.2	0.8	2.1	2.0

TABLE III. Considered reactions with corresponding cross sections σ between ions and the background gas mixture H_2 -Ar taken from Bogaerts and Gijbels³⁶ and calculated for a gas temperature of 540 K. *— σ is calculated from the corresponding rate coefficient.

k	Reaction	σ (10^{-19}m^2)	
		Ref. 36	Ref. 35*
3.1	$\text{H}^+ + \text{H}_2 \rightarrow \text{H}^+ + \text{H}_2$	9.0	
3.2	$\text{H}^+ + \text{Ar} \rightarrow \text{H}^+ + \text{Ar}$	7.9	
3.3	$\text{H}_2^+ + \text{H}_2 \rightarrow \text{H}_2 + \text{H}_2^+$	0.04	
3.4	$\text{H}_2^+ + \text{H}_2 \rightarrow \text{H}_3^+ + \text{H}$	6.6	5.5
3.5	$\text{H}_2^+ + \text{Ar} \rightarrow \text{ArH}^+ + \text{H}$	6.7	7.9
3.6	$\text{H}_2^+ + \text{Ar} \rightarrow \text{Ar}^+ + \text{H}_2$	1.2	0.8
3.7	$\text{H}_3^+ + \text{H}_2 \rightarrow \text{H}_3^+ + \text{H}_2$	7.8	
3.8	$\text{H}_3^+ + \text{Ar} \rightarrow \text{H}_3^+ + \text{Ar}$	8.8	
3.9	$\text{H}_3^+ + \text{Ar} \rightarrow \text{ArH}^+ + \text{H}_2$	0	1.6
3.10	$\text{Ar}^+ + \text{H}_2 \rightarrow \text{ArH}^+ + \text{H}$	3.5	3.3
3.11	$\text{Ar}^+ + \text{H}_2 \rightarrow \text{H}_2^+ + \text{Ar}$	0.75	0.07
3.12	$\text{Ar}^+ + \text{Ar} \rightarrow \text{Ar}^+ + \text{Ar}$	4.9	
3.13	$\text{Ar}^+ + \text{Ar} \rightarrow \text{Ar} + \text{Ar}^+$	4.8	
3.14	$\text{ArH}^+ + \text{H}_2 \rightarrow \text{ArH}^+ + \text{H}_2$	5.5	
3.15	$\text{ArH}^+ + \text{H}_2 \rightarrow \text{H}_3^+ + \text{Ar}$	1.7	2.4
3.16	$\text{ArH}^+ + \text{Ar} \rightarrow \text{ArH}^+ + \text{Ar}$	10.6	

of our rate coefficients with those of Kimura and Kasugai¹⁷ yields that $K_{1.2}$ and $K_{1.5}$ agree within 15%. In contrast, K_k with $k = 1.1, 1.3$, and 1.4 , i.e., the K 's for the electron collisions with molecular hydrogen, differ depending on T_e by a factor of 0.3 to 13 from the present K 's. Due to the fact that the here used literature source for σ_k (Ref. 29) is more recent and provides recommended values, we used these data. We note that Hjartarson *et al.* also used this data set.

2. Ion-molecule collisions

A simplified form for the rate coefficient of ion-molecule reactions (reaction k) between particle i and j is derived in the following. A special but frequent case in ion-molecule reactions is the ion-induced dipole scattering where σ_k is proportional to $E_{ij}^{-0.5}$ in the low energy range up to 1.10 eV.^{24,37} In this case, the product $\sigma_k v_{ij}$ in the integral of Eq. (4) becomes independent of energy because $\sigma_k \propto E_{ij}^{-0.5}$ and $v_{ij} = (2E_{ij}/\mu_{ij})^{0.5}$. Here, $E_{ij} = 1.5k_B T_g$ is used. As a consequence, Eq. (4) simplifies to

TABLE IV. Reaction set for excited argon with rate coefficients K for a reaction k . The electron temperature T_e is considered in eV.

k	Reaction	K (m^3s^{-1}), (s^{-1})	Reference
4.1	$\text{e}^- + \text{Ar} \rightarrow \text{Ar}_m + \text{e}^-$	$5.0 \times 10^{-15} \times e^{-12.64/T_e}$	17
4.2	$\text{e}^- + \text{Ar} \rightarrow \text{Ar}(4p) + \text{e}^-$	$2.1 \times 10^{-14} \times e^{-13.13/T_e}$	17
4.3	$\text{Ar}_m + \text{H}_2 \rightarrow 2\text{H} + \text{Ar}$	1.1×10^{-16}	17
4.4	$\text{Ar}_r + \text{H}_2 \rightarrow 2\text{H} + \text{Ar}$	1.1×10^{-16}	17
4.5	$\text{Ar}_r \rightarrow \text{Ar} + h\nu$	1.0×10^5	17
4.6	$\text{Ar}(4p) \rightarrow \text{Ar}_r + h\nu$	3.0×10^7	17
4.7	$\text{Ar}(4p) \rightarrow \text{Ar}_m + h\nu$	3.0×10^7	17
4.8	$\text{Ar}_m + \text{wall} \rightarrow \text{Ar}$	$K_{w\text{Ar}_m}$	18

$$K_k = \sigma_k(E_{ij})v_{ij}. \quad (7)$$

The used K_k 's for ion-molecule reactions are all taken from a compilation by Anicich³⁵ and are listed in Table II. Anicich provides a collection of recommended values of rate coefficients for a wealth of bimolecular ion-molecule reactions for a gas temperature of 300 K. The gas temperature in the here investigated plasma is in the range between 300 and 800 K. However, this should not significantly influence the rate coefficients due to the fact that in most cases K is independent of T_g as discussed above.

In Table II, we compare the data of Anicich³⁵ with the rate coefficients used by Kimura and Kasugai¹⁷ and Hjartarson *et al.*¹⁸ In addition, values derived from Bogaerts and Gijbels³⁶ are shown that will be used in Sec. III F 1. Hjartarson *et al.* considered all ion-molecule reactions of Table II whereas Kimura and Kasugai¹⁷ only considered reactions 2.1, 2.2, 2.6, and 2.7. In Bogaerts and Gijbels,³⁶ one can find a complete set of σ_k as function of energy. This includes elastic and inelastic scattering and ion-molecule reactions leading to production of other species. The cross sections of Bogaerts and Gijbels³⁶ are converted into rate coefficients according to Eq. (7) for the experimentally obtained $T_g = 540$ K (see Sec. II) to allow a direct comparison in Table II. Our values for $K_{2,1}$ and $K_{2,6}$ agree reasonably well with the three other references.^{17,18,36} Similarly, $K_{2,3}$ and $K_{2,4}$ agree well with the values of Hjartarson *et al.* and Bogaerts and Gijbels. The maximal deviation is a factor of 1.6, which has to be considered as rather good for rate coefficients of ion-molecule collisions. For $K_{2,2}$, Hjartarson *et al.* and Kimura and Kasugai use the same value, which is a factor of 2.4 higher than ours, whereas the value of Bogaerts and Gijbels is closer to the here used value. However, a factor of 2.4 is still a moderate deviation for rate coefficients of ion-molecule collisions. The deviation for $K_{2,5}$ is much larger. The ratio between Hjartarson *et al.* and the value used in this work is $K_{2,5}^{\text{Hjartarson}}/K_{2,5}^{\text{thiswork}} = 0.027$. The value of Bogaerts and Gijbels is even 0. The value for $K_{2,7}$ in Hjartarson *et al.* and Bogaerts and Gijbels is a factor of about 12 and that of Kimura and Kasugai a factor of 4.4 higher than our value. The influence of the used rate coefficients on the model results will be discussed in Sec. V.

F. Wall losses

The main loss process for ions and radicals in a low-temperature plasma in the pressure range from 0.1 to 10 Pa is the flux to the wall. Volume recombination is improbable in this pressure regime (see Sec. III B). For the wall loss, the discharge geometry is important because it determines the mean distance between the plasma center and the walls. Here, a cylindrical geometry is assumed with a cylinder height l and cylinder radius r . The distance between the upper and lower electrode is $l_{el} = 60$ mm. The upper and lower electrodes are circular with a radius of $r_{el} = 65$ mm, whereas the chamber has a radius of $r_{ch} = 125$ mm. The total height of the chamber is $l_{ch} = 360$ mm. Because there is no radial side wall between the upper and lower electrode at r_{el} ; and due to an aspect ratio $l_{el}/r_{el} \lesssim 1$, only axial losses to the

upper stainless steel electrode or lower quartz dome are considered. This assumption was also made in an earlier investigation describing an experiment with a comparable chamber geometry (see Appendix in Osiac *et al.*³⁸). Therefore, in the following calculations, the limit $r \rightarrow \infty$ will be applied.

1. Wall loss for ions

We assume that ions reaching the wall recombine with a probability of 1. Either they recombine directly ($H^+ + \text{wall} \rightarrow H$, $H_2^+ + \text{wall} \rightarrow H_2$, $Ar^+ + \text{wall} \rightarrow Ar$) or dissociatively ($H_3^+ + \text{wall} \rightarrow H_2 + H$, $ArH^+ + \text{wall} \rightarrow Ar + H$). For the case of dissociative recombination, the produced atomic hydrogen is assumed to be reflected from the surface with a probability of 1. The rate coefficients K_{wi} for the loss of positive ions to the walls are based on the uniform density discharge model for low and intermediate pressures of Lieberman and Lichtenberg²⁴

$$K_{wi} = \frac{A_{eff}}{V} v_{B,i}. \quad (8)$$

Here, $v_{B,i} = \sqrt{eT_e/M_i}$ denotes the Bohm velocity of an ion species i with mass M_i , $V = \pi r^2 l$ the plasma volume, and A_{eff} an effective area surrounding the plasma. A_{eff} is given by

$$A_{eff} = 2\pi r(rh_l + lh_r). \quad (9)$$

h is the ion density ratio between plasma edge and plasma center. h is different for axial (h_l) and radial (h_r) loss (Godyak³⁹)

$$h_l = \frac{0.86}{\sqrt{3 + \frac{l}{2\lambda_i}}} \quad (10)$$

and

$$h_r = \frac{0.8}{\sqrt{4 + \frac{r}{\lambda_i}}}. \quad (11)$$

As mentioned above, it is assumed that r is infinite. This implicates that h_r is zero and, therefore, that the density profile in the radial direction is flat. For our geometry, the surface-to-volume ratio yields $A_{eff}/V = 2h_l/l_{el}$.

λ_i is the mean free path length for ions traversing the background gas consisting of two species j ($j = H_2, Ar$) with density n_j

$$1/\lambda_i = \sum_{j,k} \sigma_k n_j. \quad (12)$$

σ_k denotes the cross section for the collision (reaction k) of the ion with the background gas atom or molecule. σ_k is taken from Bogaerts and Gijbels³⁶ where one can find a complete set of σ_k as function of energy. For comparison, the rate coefficients of Anicich³⁵ which are used for the volume reactions of the rate equation model are converted into cross sections according to Eq. (7). The description of the ion

diffusion through the background gas requires also data for elastic and inelastic scattering, which are not provided by Anicich.³⁵ The differences of the data set between Bogaerts and Gijbels and Anicich as shown in Table III and discussed in Sec. III E 2 have only a very low influence on the calculated λ_i . The values for individual σ_k 's are shown in Table III for $E_{ij} = 1.5 k_B T_g$ with $T_g = 540$ K as obtained experimentally (see Sec. II).

2. Wall loss for atomic hydrogen

Atomic hydrogen is lost by reactions at the chamber walls. It is described by the loss rate coefficient, which is the inverse of the loss time. The wall loss rate coefficient K_{wH} of atomic H is composed of a diffusive part K_D and a surface loss part K_s ⁴⁰

$$\frac{1}{K_{wH}} = \frac{1}{K_D} + \frac{1}{K_s} = \frac{\Lambda^2}{D_H} + \frac{V}{A_H} \frac{2(2 - \beta_H)}{\beta_H} \frac{1}{v_H} \quad (13)$$

(Λ —diffusion length, D_H —diffusion constant of H, V —plasma volume, A_H —wall area for loss of H, β_H —surface loss probability for H, and v_H —mean velocity of H).

K_D describes the diffusion to the wall. K_D is a function of Λ and D_H . The diffusion length Λ is given by⁴⁰

$$\frac{1}{\Lambda^2} = \left(\frac{\pi}{l}\right)^2 + \left(\frac{2.405}{r}\right)^2. \quad (14)$$

For our geometry with $l = l_{el}$ and $r \rightarrow \infty$, the diffusion length is $\Lambda = l_{el}/\pi$. The expression for the diffusion constant is taken from Lieberman and Lichtenberg²⁴ and extended to diffusion through a background gas, which consists of several species j

$$\frac{1}{D_H} = \sqrt{\frac{8}{\pi k_B T_H}} \sum_j \sigma_{Hj} n_j \sqrt{\mu_{Hj}}, \quad (15)$$

which is identical with Blancs law (see, e.g., Ref. 41). Here, the temperature of atomic hydrogen T_H is used because it determines the mean collisional energy of hydrogen with the background gas. The cross sections are estimated by the hard-sphere model where $\sigma_{Hj} = \pi(r_H + r_j)^2$ is calculated by the atomic hydrogen and collision partner radii r_H and r_j , respectively. For atomic hydrogen, the Bohr radius is assumed. For molecular hydrogen and argon, the radii are calculated from the gas kinetic cross sections given in Ref. 24 with the hard-sphere model, i.e., $r_{H_2} = 1.47$ Å and $r_{Ar} = 2.00$ Å.

K_s is the loss rate at the walls. K_s is a function of the surface-to-volume ratio, v_H and especially β_H . v_H is calculated by the mean velocity of atomic hydrogen: $v_H = \sqrt{8k_B T_H / \pi M_H}$ with M_H being the mass of atomic hydrogen.

In the following, we estimate the temperature of atomic hydrogen T_H . Atomic hydrogen is produced by dissociation and the atoms gain approximately half of the dissociation energy ($E_{diss} = 4.45$ eV (Ref. 34)). This energy will be dissipated by collisions with the background gas. The degree to which this energy is dissipated depends on the background pressure and, hence, on the mean number of collisions with

background gas species. Tatarova *et al.*⁴² determined the atomic hydrogen temperature in H_2 , H_2 -He, and H_2 -Ar microwave plasmas by measuring the Doppler broadening of the H_α line. Their plasma conditions were: operating pressure 30 Pa and microwave power 600 W. They found atomic hydrogen temperatures between 3000 and 4000 K depending on gas admixture. Furthermore, they measured the Doppler temperature of the He line at 667.8 nm and the rotational temperature of H_2 molecules, which ranged between 300 and 900 K. That means for their conditions, the H atom temperature was a factor of 3 to 10 higher than the gas temperature. Because our operating pressure of 1.0 Pa is considerably lower than that of Tatarova *et al.*, we have to assume that in our case, the atomic hydrogen temperature is even higher. For simplicity, we assume that in our case, the temperature of atomic hydrogen is 6000 K ($=0.52$ eV). The sensitivity of the model on this estimate will be discussed in Sec. IV C.

For low β or low pressure, K_{wH} can be approximated with K_s (see Ref. 40). For high β ($\beta \approx 1$) or high pressure, K_{wH} can be approximated with K_D (see Ref. 40). For $\beta = 1$, all hydrogen atoms reaching the wall are lost, no H returns from the surface. For high pressure, the transport to the wall determines the flux reaching the surface. If the pressure is high, the density profile is rather peaked in the center such that the density at the wall is comparatively low.

In the following, the determination of β will be discussed. In our case, the wall loss is determined by recombination ($H + \text{wall} \rightarrow 1/2 H_2$). β is material-dependent. In our experiment, the plasma interacts with two chamber wall materials: stainless steel (upper electrode) and quartz (dome containing the coil). Quartz has a low β_H around 0.001 and stainless steel a higher β_H in the range of 0.01–0.2.^{43–45} Therefore, only the area of the upper electrode is considered for the loss surface of H, i.e., $A_H = \pi r_{el}^2$. There are several ways to determine K_{wH} and especially β_H . The simplest way would be to use data of β_H from literature. Unfortunately, they vary over more than one order of magnitude and are very sensitive to the experimental set-up. Another way is to measure the loss time of H in the afterglow.^{43–45} However, this is very elaborate and will be a topic of a forthcoming publication. A third way is to derive it from the measured dissociation degree n_H^m/n_{H_2} . To do so, β_H is used as fit parameter for the rate equation system. Based on the assumption that β_H does not depend on the plasma conditions, the calculated dissociation degree density n_H^c/n_{H_2} is fitted to the measured dissociation degree n_H^m/n_{H_2} for different Ar fractions by minimizing χ^2 through a variation of β_H . Assuming Gaussian uncertainties in n_H^m/n_{H_2} the χ^2 is calculated by⁴⁶

$$\chi^2 = \sum_{f=1}^Z \left(\frac{n_{Hf}^m/n_{H_2} - n_{Hf}^c/n_{H_2}(\beta_H)}{\Delta(n_{Hf}^m/n_{H_2})} \right)^2, \quad (16)$$

where f is an index for the plasma condition, Z is the total number of considered values ($Z=4$ for the case considered here), and $\Delta(n_H^m/n_{H_2})$ is the error of the measured dissociation degree. Because T_e (see Sec. III D) is practically independent of n_H^c/n_{H_2} , first the quasi-neutrality and, therefore, T_e are calculated. Because the production rate for H strongly

depends on T_e , the $n_{\text{H}}^{\text{c}}/n_{\text{H}_2}$ fitting procedure is performed after calculating T_e .

G. Excited Argon

To assess whether or not metastable argon Ar_m influences the dissociation of hydrogen, Ar_m is included in the model. To do this, a simplified collisional radiative model is applied.¹⁷ This model takes into account only the most relevant electronically excited states. Here, Ar_m designates the excited Ar levels $1s^5$ and $1s^3$ in Paschen's notation. Similarly, Ar_r designates the excited Ar species in the $1s^4$ and $1s^2$ levels and $\text{Ar}(2p)$ the excited Ar species in the $2p^{10}$ to $2p^1$ level. The considered reactions are summarized in Table IV. They are based on the reaction set of Kimura and Kasugai.¹⁷ Kimura and Kasugai take into account 18 reactions for the excited Ar states. In a preceding study, we found that this reaction set can be reduced to the 8 reactions shown in Table IV. These 8 reactions are the dominant ones, which are sufficient to calculate the metastable Ar density n_{Ar_m} (see Ref. 47). Other reactions of excited Ar, such as the reaction $\text{Ar}_m + \text{Ar}_m \rightarrow \text{Ar}^+ + \text{Ar} + e^-$, are not relevant for our plasma conditions due to the low pressure. However, for pressures higher than 1 Pa, this reaction cannot be neglected.^{48,49} For the wall loss of Ar_m , Eq. (13) is used with the corresponding values for Ar_m , i.e., $\beta_{\text{Ar}_m} = 1$ (see Ref. 18).

IV. MODEL RESULTS

The calculations are made exactly for the plasma conditions applied in the experiment (see Sec. II). In addition, results for very low and very high Ar fraction are calculated, namely $f_{\text{Ar}} = 5\%$, 87% and 95% . For these additional Ar fractions, n_e is required as input parameter in the model. It was determined by linear interpolation between neighboring measured values of n_e .

A. Ion chemistry

The most important reactions for the production of ions in a low-temperature plasma are the ionization by inelastic electron collisions with the background gas. In our case, the background gas consists of H_2 and Ar. The corresponding primary ions are H_2^+ and Ar^+ . A small contribution (percent range) of atomic H^+ ions is also produced as primary ions. One would expect that H_2^+ and Ar^+ are also the dominant ion species in a H_2 -Ar low-temperature plasma. However, measurements have shown that H_3^+ and ArH^+ are dominant.¹⁶ H_3^+ and ArH^+ can only be produced by ion-molecule collisions in the plasma volume.

For a better insight into the reaction chemistry in a H_2 -Ar plasma, we will discuss the total production rates using $R_{\text{tot}}^{\text{IG}}$. The losses will be discussed using the total loss frequency $\nu_{\text{tot}}^{\text{IL}}$. $R_{\text{tot}}^{\text{IG}}$ and $\nu_{\text{tot}}^{\text{IL}}$ are calculated from the model results by summing up all contributions k and \tilde{k} that contribute to gain or loss of the species i , respectively. To identify the dominant reactions, the individual production rates R_k^{IG} and loss frequencies ν_k^{IL} as well as $R_{\text{tot}}^{\text{IG}}$ and $\nu_{\text{tot}}^{\text{IL}}$ for all investigated ions are presented in Fig. 3. The ion chemistry for ArH^+ will be discussed in some detail; while for the other ions, only the most important results are briefly mentioned.

1. ArH^+

To explain the dependence of the ArH^+ density on f_{Ar} , the ion density n_{ArH^+} , the production rates $R_{\text{tot}}^{\text{ArH}^+ \text{G}}$, and loss frequencies $\nu_{\text{tot}}^{\text{ArH}^+ \text{L}}$ are shown in Figs. 3(a) and 3(b), respectively. n_{ArH^+} has a maximum with a value of $1.5 \times 10^{16} \text{m}^{-3}$ for f_{Ar} between about 50% and 80% and is 0 for pure H_2 and pure Ar. The total production rate $R_{\text{tot}}^{\text{ArH}^+ \text{G}}$ shows a maximum for f_{Ar} between about 30% and 50%. The dominant contribution to $R_{\text{tot}}^{\text{ArH}^+ \text{G}}$ comes from reaction 2.6 ($\text{Ar}^+ + \text{H}_2 \rightarrow \text{ArH}^+ + \text{H}$), which accounts for at least 2/3 of the total production rate. As a consequence, the ArH^+ ion density strongly depends on n_{Ar^+} . Reactions 2.3 ($\text{H}_2^+ + \text{Ar} \rightarrow \text{ArH}^+ + \text{H}$) and 2.5 ($\text{H}_3^+ + \text{Ar} \rightarrow \text{ArH}^+ + \text{H}_2$) provide minor contributions to $R_{\text{tot}}^{\text{ArH}^+ \text{G}}$. The total loss frequency $\nu_{\text{tot}}^{\text{ArH}^+ \text{L}}$ (see Fig. 3(b)) decreases linearly with increasing f_{Ar} . Therefore, the maximum of n_{ArH^+} is shifted to higher Ar fractions compared to the production rate. $\nu_{\text{tot}}^{\text{ArH}^+ \text{L}}$ consists of the linearly decreasing $\nu_{2.2}$ due to reaction 2.2 and the constant wall loss frequency ν_{wArH^+} . For $f_{\text{Ar}} \leq 60\%$, the dominant loss process is due to reaction 2.2; while for higher f_{Ar} , the loss of ArH^+ to the wall dominates. ν_{wArH^+} is roughly constant over the whole mixture range because it depends on the geometry of the plasma vessel and the square root of T_e (see Eq. (8)). T_e changes only slightly (see Sec. IV B). The dependence of n_{ArH^+} on f_{Ar} is similar to $R_{\text{tot}}^{\text{ArH}^+ \text{G}}$.

2. Ar^+

For Ar^+ , the ion density n_{Ar^+} , the production rates $R_{\text{tot}}^{\text{Ar}^+ \text{G}}$, and loss frequencies $\nu_{\text{tot}}^{\text{Ar}^+ \text{L}}$ are shown in Figs. 3(c) and 3(d), respectively. The total production rate $R_{\text{tot}}^{\text{Ar}^+ \text{G}}$ increases for $0 \leq f_{\text{Ar}} \leq 30\%$, then stays roughly constant, and slightly decreases for $f_{\text{Ar}} > 70\%$. The production of Ar^+ is almost exclusively due to electron-induced ionization with rate $R_{1.5}$ ($e^- + \text{Ar} \rightarrow \text{Ar}^+ + 2e^-$). The total loss frequency $\nu_{\text{tot}}^{\text{Ar}^+ \text{L}}$ decreases linearly by a factor of 5 with increasing f_{Ar} . Again, the wall loss is roughly constant over the whole mixture range, while the loss due to reaction 2.6 ($\text{Ar}^+ + \text{H}_2 \rightarrow \text{ArH}^+ + \text{H}$) decreases linearly with increasing Ar fraction. The contribution of reaction 2.7 ($\text{Ar}^+ + \text{H}_2 \rightarrow \text{Ar} + \text{H}_2^+$) to the loss of Ar^+ can be neglected. n_{Ar^+} increases roughly linearly from 0 for pure H_2 to $3.1 \times 10^{16} \text{m}^{-3}$ for pure Ar. For $5 < f_{\text{Ar}} < 30\%$, this is attributed to the increase in $R_{\text{tot}}^{\text{Ar}^+ \text{G}}$ which is mainly due to the increase in f_{Ar} . For $f_{\text{Ar}} > 30\%$, the increase of n_{Ar^+} is mostly due to the decreasing loss rate.

3. H_3^+

The density and rates for H_3^+ are shown in Figs. 3(e) and 3(f). The total production rate $R_{\text{tot}}^{\text{H}_3^+ \text{G}}$ and the density $n_{\text{H}_3^+}$ show a maximum at $f_{\text{Ar}} = 12.6\%$. For the production of H_3^+ , two reactions are important: First, reaction 2.1 ($\text{H}_2^+ + \text{H}_2 \rightarrow \text{H}_3^+ + \text{H}$, see Table I) with rate $R_{2.1}$ which is the dominant process up to $f_{\text{Ar}} \approx 25\%$. Second, reaction 2.2 with rate $R_{2.2}$ ($\text{ArH}^+ + \text{H}_2 \rightarrow \text{H}_3^+ + \text{Ar}$) which is the dominant channel for $f_{\text{Ar}} > 25\%$. The total loss frequency $\nu_{\text{tot}}^{\text{H}_3^+ \text{L}}$ stays roughly constant for all Ar fractions. The loss is mainly due to recombination on the wall.

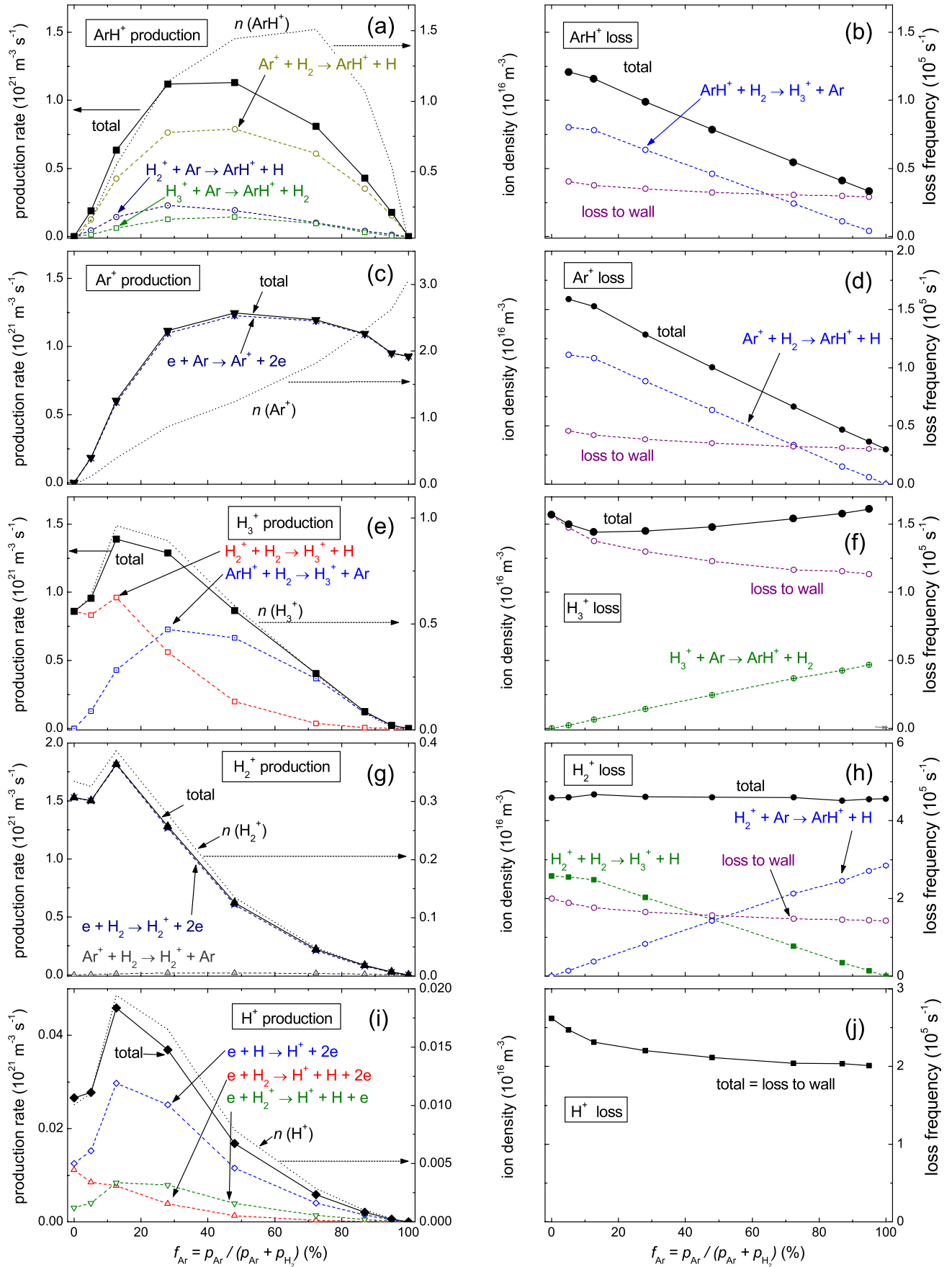


FIG. 3. Left column: production rates (left-hand scale) and ion densities (right-hand scale; dotted lines) for the ion species ArH^+ (a), Ar^+ (c), H_3^+ (e), H_2^+ (g), and H^+ (i), respectively. Right column: loss frequencies for the ion species ArH^+ (b), Ar^+ (d), H_3^+ (f), H_2^+ (h), and H^+ (j), respectively. Contributions lower than 5% are not shown.

4. H_2^+

The data for H_2^+ are presented in Figs. 3(g) and 3(h). The total production rate $R_{tot}^{H_2^+G}$ has a maximum at $f_{Ar} = 12.6\%$. $n_{H_2^+}$ is $3.3 \times 10^{15} m^{-3}$ for pure H_2 has a maximum of $3.9 \times 10^{15} m^{-3}$ at $f_{Ar} \leq 12.6\%$, and decreases monotonically to 0 for $12.6 \leq f_{Ar} \leq 100\%$. $n_{H_2^+}$ shows essentially the identical behavior as $R_{tot}^{H_2^+G}$ on f_{Ar} because the total loss frequency $\nu_{tot}^{H_2^+L}$ stays constant for all Ar fractions. H_2^+ is almost exclusively produced by electron-induced ionization from H_2 with rate $R_{1,3}$ ($e^- + H_2 \rightarrow H_2^+ + 2e^-$). The loss of H_2^+ comprises three contributions. First, reaction 2.1 ($H_2^+ + H_2 \rightarrow H_3^+ + H$) with loss frequency $\nu_{2,1}$. Second, reaction 2.3 with loss frequency $\nu_{2,3}$ ($H_2^+ + Ar \rightarrow ArH^+ + H$). Third, the loss to the wall with loss frequency $\nu_{wH_2^+}$.

In the following, two peculiarities of the studied H_2 -Ar plasma will be discussed and explained. The first peculiarity is the fact that the densities of $n_{H_2^+}$ and $n_{H_3^+}$ are considerably lower than those of n_{ArH^+} and n_{Ar^+} . While the production rates R_{tot}^G for $n_{H_2^+}$ and $n_{H_3^+}$ are comparable to the production rates for ArH^+ and Ar^+ , the absolute loss rates for H_2^+ and H_3^+ are considerably higher than those for ArH^+ and Ar^+ due to the high wall loss. The wall loss frequency $\nu_{wi}^+ = K_{wi} \propto 1/\sqrt{M_i}$ (see Eq. (8)) for H_2^+ and H_3^+ is by a factor of about $\sqrt{M_{Ar^+}/M_{H_2^+}} \approx 5$ ($x = 1, 2, 3$) higher than the corresponding value for ArH^+ and Ar^+ , and as consequence, the corresponding ion densities are lower. The second peculiarity is that $n_{H_2^+}$ is considerably lower than $n_{H_3^+}$ and n_{ArH^+} although the total production rates have roughly the same value. But in contrast to H_3^+ and ArH^+ , $\nu_{tot}^{H_2^+L}$ is much higher than the total loss frequencies of all other considered ion species. The loss of H_2^+ is not only determined by the loss to the wall, such as the loss of H_3^+ (see Fig. 3(e)), but also by the conversion to H_3^+ for low f_{Ar} (reaction 2.1) and ArH^+ for high f_{Ar} (reaction 2.3). In fact, the rate coefficients for these two reactions are those with the highest values in Table II.

5. H^+

Finally, the data for H^+ are plotted in Figs. 3(i) and 3(j). n_{H^+} is $1.0 \times 10^{14} m^{-3}$ for pure H_2 has a maximum at $f_{Ar} \leq 12.6\%$ and decreases monotonically to 0 for $12.6 \leq f_{Ar} \leq 100\%$. The total production rate $R_{tot}^{H^+G}$ is about a factor of 50 lower than the total production rate of H_2^+ but the dependence on f_{Ar} is very similar to that of H_2^+ . For the production of H^+ , three reactions are important: First, direct ionization of atomic hydrogen (reaction 1.2, see Table I) with rate $R_{1,2}$. Second, dissociative ionization of molecular hydrogen (reaction 1.4) with rate $R_{1,4}$. Third, dissociation of H_2^+ (reaction 1.6) with rate $R_{1,6}$. The total loss frequency $\nu_{tot}^{H^+L}$ decreases by 20% with increasing f_{Ar} . The only significant loss process for H^+ is recombination on the wall. The dependence of n_{H^+} on f_{Ar} is accordingly fully determined by the total production rate $R_{tot}^{H^+G}$.

n_{H^+} has a considerably lower density than $n_{H_2^+}$ ($n_{H^+}/n_{H_2^+} \approx 0.05$). This is explained as follows. While H^+ is produced by direct ionization of atomic hydrogen (reaction 1.2) and by dissociative ionization of molecular hydrogen

(reaction 1.4), H_2^+ is produced by direct ionization of molecular hydrogen (reaction 1.3: $e^- + H_2 \rightarrow H_2^+ + 2e^-$). The rate coefficients $K_{1,2}$ and $K_{1,3}$ for the two direct ionization processes have similar values. The main difference with respect to the corresponding production rates originates from the different densities of atomic and molecular hydrogen. The dissociation degree n_H/n_{H_2} is low ($\approx 2\%$, see Sec. IVC) and, therefore the ratio of the production rates is of the same order of magnitude. Furthermore, reactions 1.4 and 1.3 are both proportional to the molecular hydrogen density, but the rate coefficients $K_{1,4}$ and $K_{1,3}$ are considerably different ($K_{1,4}/K_{1,3} < 0.01$). Therefore, the production rate of H^+ according to reaction 1.4 is comparable to $R_{1,2}$.

B. Electron temperature

As described in Sec. IIID in our model, T_e is fitted to fulfill the quasi-neutrality condition. The measured (Ref. 16) and fitted electron temperatures are plotted in Fig. 4 as a function of f_{Ar} . The measured T_e of the pure hydrogen plasma is 5.2 eV. In the H_2 -Ar plasma, the measured T_e decreases monotonically reaching 2.9 eV for the pure Ar plasma. The modeled T_e shows the same behavior as the measured T_e but yields systematically higher values. This deviation ranges between 0.3 and 0.8 eV. All in all, the rate equation model describes T_e quite well. We interpret the good agreement of fitted and measured T_e as an indication that the electron temperature is mostly determined by the rate equations or, more precisely, by the particle balance and not by the power balance. A similar conclusion has been drawn earlier by Tao *et al.*²⁶ The electron density is, on the other hand, determined by the power balance.²⁶

The decrease of T_e with increasing f_{Ar} was discussed in our previous work.¹⁶ The observed decrease of T_e was attributed to the increasing effective ion mass with increasing f_{Ar} . The effective ion mass increases monotonically from 2.7 amu for a pure H_2 plasma to 40 amu for a pure Ar plasma.

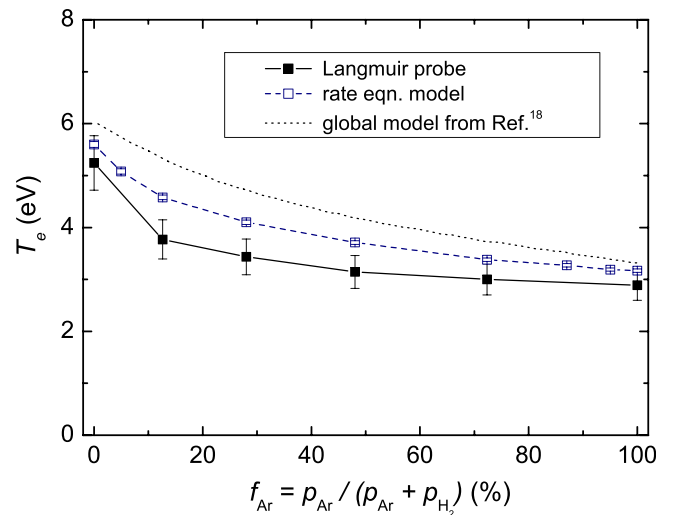


FIG. 4. Measured (closed symbols) and modeled (open symbols) electron temperatures as a function of f_{Ar} for a total pressure of 1.0 Pa. The results of this work are compared with the results (dotted line) of a global model calculated by Hjartarson *et al.*¹⁸ for a H_2 -Ar plasma with the following input parameters: $p = 0.91$ Pa, $l = 0.076$ m, $r = 0.152$ m, and $T_g = 500$ K.

We compare our results for T_e with those of the global model by Hjartarson *et al.*¹⁸ which are shown as dashed lines in Fig. 4. The input parameters of Hjartarson *et al.* are comparable to the input parameters of the present work. They used the following input parameters: pressure $p = 0.91$ Pa, gas temperature $T_g = 500$ K, and dimensions $l = 0.076$ m and $r = 0.152$ m. Their calculated T_e for the pure hydrogen plasma is 6.0 eV. In the H_2 -Ar plasma, it decreases monotonically reaching 3.3 eV for the pure Ar plasma. The T_e of Hjartarson *et al.* is qualitatively similar to our data but shifted to slightly higher values (see Fig. 4). The minimum and maximum differences are 0.2 and 0.7 eV. This difference can, however, not be attributed to the slightly different plasma parameters. Their pressure and gas temperature are about 10% lower than our values. But because the determining parameter is the gas density, these two changes cancel out and result in the same density. The geometry is slightly different. Their l is about 25% larger than our value. However, inserting their geometry in our model results in an slightly lower calculated T_e , thus increasing the difference between Hjartarsons and our values. Therefore, the change in geometry cannot explain the difference. We assume that the difference of the calculated T_e values is due to the used reaction set and rate constants. Summarizing, the T_e of our model is in reasonable agreement with the literature on the one hand and with our measured values on the other hand.

C. Dissociation degree and surface loss probability of H

The measured (Ref. 16) and fitted hydrogen dissociation degrees n_H/n_{H_2} are shown in Fig. 5. The measured dissociation degree stays nearly constant over the considered Ar fraction range with a mean value of $(1.7 \pm 0.4)\%$. n_H^c/n_{H_2} starts at 0.8% for the pure H_2 plasma case and increases up to 1.6% for $f_{Ar} = 12.6\%$. In the range $12.6 \leq f_{Ar} \leq 72.3\%$, n_H^c/n_{H_2} stays roughly constant with values between 1.5% and 2.0% in accordance with the measured data. As described in Sec. III F 2, in our model, the calculated

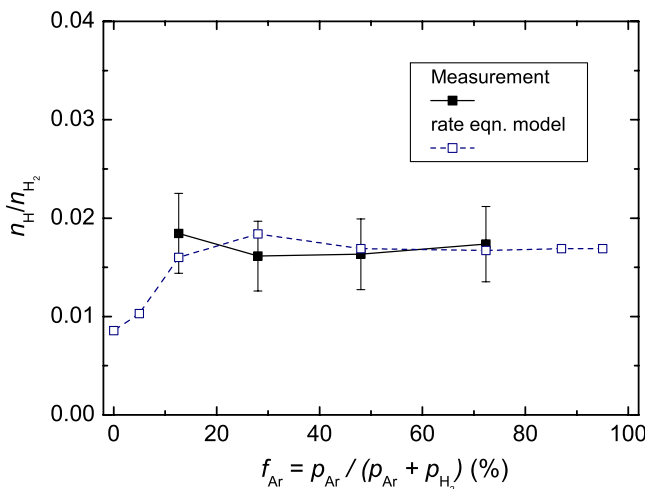


FIG. 5. Measured (closed symbols) and modeled (open symbols) dissociation degree of hydrogen n_H/n_{H_2} as a function of the Ar fraction f_{Ar} . The calculated curve was fitted with a surface loss probability of atomic hydrogen on stainless steel of $\beta_H = 0.24$.

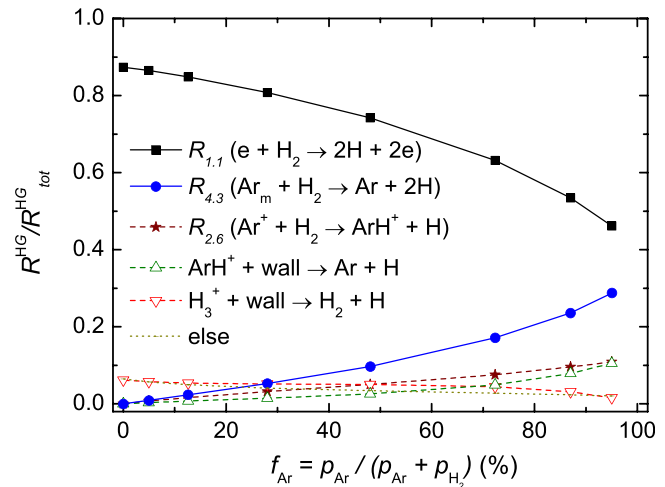


FIG. 6. Relative production rates R^{HG}/R_{tot}^{HG} as a function of the argon fraction f_{Ar} for atomic hydrogen. Contributions to R_{tot}^{HG} of lower than 5% are combined in “else.”

dissociation degree n_H^c/n_{H_2} is fitted to the measured values n_H^m/n_{H_2} by minimizing χ^2 through a variation of β_H .

To illustrate the most important reactions for atomic hydrogen, the relative reaction rates for the production of H are shown in Fig. 6. The dominant contribution to the total production rate of H R_{tot}^{HG} comes from the dissociation of H_2 by electron collisions (reaction 1.1). The contribution is high for low Ar fractions and decreases to a value of $R_{1,1}^{HG}/R_{tot}^{HG} = 0.46$ for $f_{Ar} = 95\%$. Ion recombination on the wall and reaction 2.6 ($Ar^+ + H_2 \rightarrow ArH^+ + H$) contribute only little to R_{tot}^{HG} . For high Ar fractions ($f_{Ar} \geq 72.3\%$), another gain process besides the dissociation by electron collision comes into play, namely the dissociation of H_2 by the metastable Ar_m (reaction 4.3 with $R_{4,3}$). The fraction $R_{4,3}^{HG}/R_{tot}^{HG}$ for the production of H is 0.17 for $f_{Ar} = 72.3\%$ and 0.29 for $f_{Ar} = 95\%$. For comparison, for $f_{Ar} \leq 48\%$, this contribution is lower than 0.1. The Ar_m density is about 0.001-0.002 of the Ar density and is constant with f_{Ar} . We would like to note that the reaction set for the excited Ar species was included in the model to study whether there is an influence of the metastable argon Ar_m on the dissociation of hydrogen or not. To conclude, Ar_m has a noticeable influence and increases monotonically with increasing f_{Ar} but only for high Ar fractions $f_{Ar} \geq 72.3\%$ metastable, Ar influences the atomic hydrogen density markedly. In the global model of Hjartarson *et al.*,¹⁸ the metastable Ar was included but unfortunately no dissociation of H_2 with Ar_m was reported.

The only significant loss process for atomic hydrogen is recombination on the wall. The appropriate rate coefficient is K_{wH} . For our conditions, i.e., low pressure of the background gas, K_{wH} can be approximated with K_s (see Sec. III F 2) where the loss probability β_H at the surrounding chamber wall is the determining parameter.^{17,18,40} The higher β_H , the higher is the wall loss.

In the following, we try to illustrate why n_H/n_{H_2} is independent on f_{Ar} in our case. With a simplified description of the dissociation degree, its dependence on f_{Ar} is illustrated. We restrict ourselves to the two dominant processes. The production process is the dissociation of H_2 by electron

collision (reaction 1.1) with the corresponding second order rate coefficient $K_{1,1}$. The loss process is the loss of hydrogen atoms to the wall with the appropriate first order rate coefficient K_s . In steady state, the dissociation degree yields

$$\frac{n_H}{n_{H_2}} \approx \frac{2n_e \times K_{1,1}(T_e)}{K_s(\beta_H)} = 2n_e \times 8.4 \times 10^{-14} T_e^{-0.45} e^{-11.18/T_e} \times \frac{2(2 - \beta_H)l_{el}}{\beta_H} \sqrt{\frac{\pi M_H}{8k_B T_H}}. \quad (17)$$

The dissociation degree is proportional to the electron density and the rate coefficient for electron-impact dissociation. This rate coefficient is very sensitive to the electron temperature, which decreases with increasing Ar fraction (see Fig. 4). It decreases from $K_{1,1}(T_e^c = 4.3 \text{ eV}) = 3.3 \times 10^{-15} \text{ m}^3 \text{ s}^{-1}$ for $f_{Ar} = 12.6\%$ to $K_{1,1}(T_e^c = 3.3 \text{ eV}) = 1.7 \times 10^{-15} \text{ m}^3 \text{ s}^{-1}$ for $f_{Ar} = 72.3\%$. On the other hand, n_e increases from $2.3 \times 10^{16} \text{ m}^{-3}$ for $f_{Ar} = 12.6\%$ to $3.7 \times 10^{16} \text{ m}^{-3}$ for $f_{Ar} = 72.3\%$ (see Fig. 2). K_s depends strongly on the surface loss probability β_H , the surface to volume ratio $A_H/V = 1/l_{el}$, and the mean velocity of the hydrogen atoms v_H : $K_s = \beta_H / (2 \times (2 - \beta_H)) \times A_H/V \times v_H$. All these parameters determining K_s are independent of n_e , T_e , and gas density. As a consequence, the decrease of $K_{1,1}$ due to the decreasing T_e is to a large extent compensated by the increase of n_e such that the dissociation degree remains roughly constant.

The calculated values of n_H^c/n_{H_2} in Fig. 5 were achieved by varying β_H to minimize χ^2 considering all measured values of n_H^m/n_{H_2} (4 mixed plasma cases). The β_H resulting from this fit is 0.24. We would like to emphasize that this value for β_H is obtained from the full model with consideration of all possible gain and loss processes of H outlined in Sec. III and not from the simplified description leading to Eq. (17). We further note that β_H sensitively depends on the assumptions about A_H/V and $\sqrt{T_H}$ (see Sec. III F2). In this work, $T_H = 6000 \text{ K}$ is assumed. If T_H would be set to $10\,000 \text{ K}$ (2000 K), the resulting β_H would be 0.18 (0.40).

The error was determined from the probability distribution of β_H . Based on the measurements of n_H^m/n_{H_2} , the probability distribution of β_H can be derived using the simplified description of the dissociation degree, i.e., Eq. (17). It does not include the error associated with T_H . Since in Eq. (17), β_H enters in the denominator the probability distribution function of β_H is asymmetric around the mode; for that reason, the uncertainties of the parameter are also asymmetric. For the 68% interval (1- σ -level), we get a relative error of +15% and -7% for β_H . Summarizing, β_H ranges from 0.22 to 0.28 with the most probable value $\beta_H = 0.24$ for the investigated H₂-Ar plasma at 1.0 Pa.

The here determined value for $\beta_H = 0.24$ for a stainless steel surface is in the range of the values published by Jolly and Booth⁴⁴ and Kae-Nune *et al.*⁴⁵ In these works, β_H was determined experimentally from time-resolved H density measurements in the afterglow. The experimentally obtained values for β_H range between 0.13 ± 0.02 ($p = 67 \text{ Pa}$, Ref. 44) and 0.20 ± 0.05 ($p = 40 \text{ Pa}$, Ref. 45). However, our β_H differs significantly from the values used in the global models by Kimura and Kasugai¹⁷ and Hjartarson *et al.*,¹⁸ where a value for β_H of 0.02 was used.

D. Model sensitivity

The sensitivity of the model result on the five input parameters was studied and is summarized in Table V. In each line of Table V, one model input parameter is varied while the other parameters are kept constant. Each of these five parameters is increased or decreased by a factor of 2 and the corresponding influence on the listed model results is shown relative to the normalized values from line three of the table. The varied input parameters and their variations are listed in column 1 of Table V. The influence of these variations on the following output parameters is shown: normalized ion densities, dissociation degree, and T_e . The procedure for obtaining T_e which is described in Sec. III is unchanged except for the situation where this parameter is varied to study its sensitivity. These variations were carried out for all investigated Ar fractions, but in Table V only the case for $f_{Ar} = 48\%$ is shown. The results for the other investigated Ar fractions in a range of $20 < f_{Ar} < 80\%$ are in general rather similar to the results for $f_{Ar} = 48\%$.

First, we investigate the influence of β_H on the model results. The numbers in the body of Table V are the relative changes of the values shown in line three. A relative value of 1.00 means that the values are not changed. We can see that only n_{H^+}/n_e and n_H/n_{H_2} are strongly influenced by β_H . This is due to the fact that the density of H is nearly inversely proportional to β_H and n_{H^+} is to a large extent produced by direct ionization of atomic hydrogen. As a consequence, the neutral and ionic hydrogen atom densities are strongly correlated. Because the contribution of the H^+ ion density to the total ion density is negligible and the other ion densities are unchanged, the plasma density does not change and

TABLE V. The sensitivity of the model with respect to variation of the input parameters. Considered is the H₂-Ar plasma with a total pressure of 1.0 Pa and an Ar fraction of $f_{Ar} = 48\%$. The input parameters with their original values and the corresponding output values are shown in the third line. In the following lines are the relative changes of the values shown in line three for the variation of one input parameter as indicated in column 1.

Input	Output						T_e^c
	$\frac{n_{ArH^+}}{n_e}$	$\frac{n_{Ar^+}}{n_e}$	$\frac{n_{H_3^+}}{n_e}$	$\frac{n_{H_2^+}}{n_e}$	$\frac{n_{H^+}}{n_e}$	$\frac{n_H}{n_{H_2}}$	
$\beta_H = 0.24$ $n_e = 3.1 \times 10^{16} \text{ m}^{-3}$ $T_e = 3.85 \text{ eV}$ $l_{el} = 0.06 \text{ m}$ $T_g = 540 \text{ K}$							
	relative values						
$2 \times \beta_H$	1.00	1.00	1.00	1.00	0.53	0.47	1.00
$0.5 \times \beta_H$	1.00	1.00	1.00	1.00	1.94	2.07	1.00
$2 \times n_e$	1.00	1.00	1.00	1.00	1.90	2.00	1.00
$0.5 \times n_e$	1.00	1.00	1.00	1.00	0.55	0.50	1.00
$2 \times T_e$	0.94	1.18	0.72	1.07	3.03	4.88	...
$0.5 \times T_e$	1.03	0.83	1.32	0.88	0.12	0.05	...
$2 \times l_{el}$	1.03	0.57	1.93	0.58	1.82	1.41	0.86
$0.5 \times l_{el}$	0.80	1.47	0.41	1.44	0.62	0.69	1.19
$2 \times T_g$	0.78	1.50	0.39	1.46	0.82	0.99	1.20
$0.5 \times T_g$	1.02	0.51	2.08	0.53	1.28	0.93	0.84

correspondingly a variation of β_H has no influence on T_e in our model.

A variation of n_e has a comparable effect on the model output results as the variation of β_H . As shown in Eq. (17), the dissociation degree is proportional to n_e and as a consequence n_H/n_{H_2} and, therefore, also n_{H^+}/n_e are strongly influenced.

A variation in T_e by a factor of 2, which is a rather dramatic change for a low-temperature plasma, causes a relatively moderate change of the normalized ion densities of ArH^+ , Ar^+ , H_3^+ , and H_2^+ . The largest deviations occur for $n_{H_3^+}$, which decreases to 0.72 if T_e is doubled and increases to 1.32 if T_e is divided by two. Although the normalized ion densities do not change significantly, the absolute ion densities change by approximately a factor of 10 if T_e is varied by a factor of 2. It has to be further noted here that a change in T_e violates the quasi-neutrality condition, i.e., the total ion density is not equal to the electron density for this specific condition. The dissociation degree n_H/n_{H_2} shows a strong dependence on T_e . As shown in Eq. (17), the dissociation degree is proportional to $K_{1,1}(T_e)$ and as a consequence n_H/n_{H_2} and, therefore, also n_{H^+}/n_e are strongly influenced. $K_{1,1}$ is proportional to $e^{-E_{1,1}/T_e}$ and is, therefore, very sensitive to a change in T_e . In fact, the relative changes of n_H/n_{H_2} and n_{H^+}/n_e are the largest changes occurring in this sensitivity study.

A variation in the cylinder height l_{el} , which corresponds to a change of the surface to volume ratio of the plasma, influences the normalized ion densities considerably. For example, if l_{el} is doubled the density of the primary ion species (Ar^+ and H_2^+) decreases to about one half of the initial value. On the other hand, the density of the secondary ion species ArH^+ and H_3^+ , which can only be produced by ion-molecule collisions in the plasma volume, is higher than the original value. This is due to the fact that the mean distance for the primary ions to the wall increases and, therefore, more primary ions are converted to secondary ions by ion-molecule reactions. This results in a higher density of ArH^+ and H_3^+ . For the inverse case, if l_{el} is divided by two, the relative contribution of the primary ions increases and that of the secondary ions decreases. The variation in l_{el} has also a substantial impact on the electron temperature. For the investigated cases, T_e varies by about 20%, which is a significant change in a low-temperature plasma. The dissociation degree n_H/n_{H_2} increases by a factor of 1.41 if l_{el} increases by a factor of 2. As shown in Eq. (17), n_H/n_{H_2} is proportional to $1/K_s \propto l_{el}$. However, in the model, this proportionality to l_{el} is partially compensated by the change in T_e .

A decrease in T_g by a factor of 2 has a comparable effect on the ion densities as an increase in l_{el} by a factor of 2. This is due to the fact that a lower T_g increases the density of the background gas $n = p/(k_B T_g)$ and, hence, increases the rate of ion-molecule reactions of the primary ions resulting in a higher density of ArH^+ and H_3^+ .

V. DISCUSSION

The novel feature of the present work is that all relevant ion densities were determined experimentally (see Ref. 16) such that a quantitative comparison to model results is

possible. Accordingly, a model was developed for this experimentally investigated discharge. The differences between the here applied model and a global model which is often used (see, e.g., Refs. 17 and 18) are: First, the electron density is provided as input parameter because the power balance is disregarded. Second, only axial losses to the upper electrode or lower quartz dome are assumed because there is no radial side wall between the upper and lower electrode at r_{el} and because of an aspect ratio $l_{el}/r_{el} \lesssim 1$. Third, β_H is determined by a fit procedure (see Sec. III F 2) because published β_H values show a significant scatter.

Kimura and Kasugai¹⁷ and Hjartarson *et al.*¹⁸ theoretically studied inductively coupled H_2 -Ar plasmas applying a global model to derive ion densities. For the variation of ion densities with changing argon fraction, both publications show in principle rather similar trends. Hjartarson *et al.*¹⁸ study the H_2 -Ar plasma in a wider parameter range and provide more detail in the description of the ion chemistry. Therefore, we compare our calculations to their modeling results. Because they were aiming at the H^- density, they included vibrationally excited H_2 which is known as precursor for the production of H^- . For a pressure variation of a H_2 -Ar plasma with $f_{\text{Ar}} = 50\%$ between 0.13 and 13 Pa, they showed normalized reaction rates and the total production and loss rates for H_3^+ and ArH^+ , which agree very well with our results. In our model, the recombination of ArH^+ with H^- was not considered. The results of Hjartarson *et al.* show that this process has only a minor contribution to $R_{\text{tot}}^{\text{ArH}^+L}$. It can reach 20% at $f_{\text{Ar}} = 50\%$. In Fig. 4, our results for T_e are compared with those of Hjartarson *et al.* also showing satisfactory agreement. Overall, our model results regarding the ion chemistry and T_e agree well with those of Hjartarson *et al.* although they additionally considered vibrationally excited $\text{H}_2(v)$ and H^- . From this, we conclude that H^- and $\text{H}_2(v)$ are not crucial for the description of the positive ion densities.

Our model results for n_{H^+} as well as n_H are clearly lower than the values of Hjartarson *et al.*¹⁸ as well as those of Kimura and Kasugai.¹⁷ This is attributed to the different values used for β_H (this work: $\beta_H = 0.24$, value of Hjartarson *et al.*¹⁸ and Kimura and Kasugai:¹⁷ $\beta_H = 0.02$). The model shows that n_{H^+} is directly related to n_H . A low n_H results in a low n_{H^+} and vice versa. In the experiment used for comparison,¹⁶ two completely independent diagnostic methods were used to measure n_H and n_{H^+} . n_H was measured by optical emission spectroscopy and the ratio of n_{H^+} to n_e was based on measurements with the plasma monitor. So it is fair to consider the data for n_H and n_{H^+} as independent measurements. In our model evaluation, n_H is used to fit β_H . The good agreement between the measured and modeled values for n_{H^+} (see below) can be regarded as an independent confirmation of the derived value for β_H .

In Fig. 7, the modeled ion densities from Fig. 3 are compared with the measured values from Ref. 16, which were also shown in Fig. 2. The calculated Ar^+ density shows the same behavior as the measured values and is very close to the absolute values of the measured curve. The modeled ArH^+ density shows a similar characteristic as the measured curve but is a factor of about 2 lower. For the pure hydrogen plasma, the dominant ion species is the H_3^+ ion with a

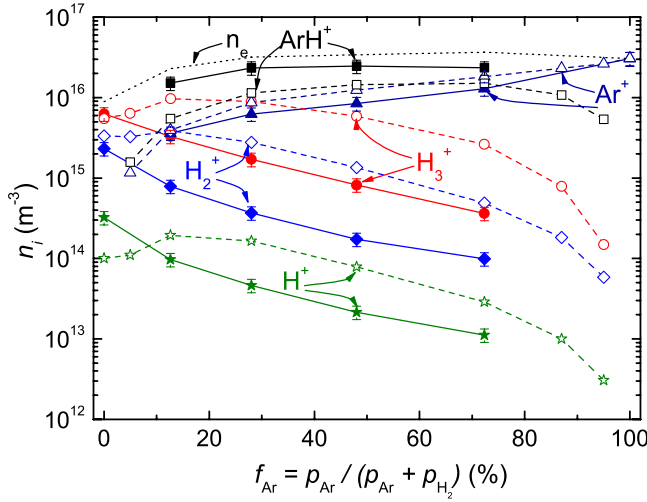


FIG. 7. Comparison of measured (closed symbols) and modeled (open symbols) ion densities and electron density as a function of the Ar fraction f_{Ar} for a total pressure of 1.0 Pa.

calculated density of $5.5 \times 10^{15} \text{ m}^{-3}$. H_2^+ and H^+ show a 1.6 times and 55 times lower calculated density than H_3^+ , respectively. The modeled H_3^+ and H_2^+ densities fit the measured densities for the pure H_2 plasma reasonably well, but clearly overestimate the measured densities by a factor of about 5 for the mixed plasma case. The calculated H^+ density behavior is similar to that of H_3^+ and H_2^+ , but the absolute values are closer to the measured ones than for H_3^+ and H_2^+ .

All in all, our model describes the experimental results of Ref. 16 reasonably well. The main features, i.e., the qualitative abundance of the ion species, the ion density dependence on the Ar fraction, and the electron temperature as function of f_{Ar} , are reproduced by the model. However, there are quantitative deviations between model and experiment. The two main deviations will be discussed in the following: First, the deviations of the calculated and measured H_3^+ and H_2^+ densities. The model overestimates the measurement by a factor of about 5 for the considered mixed H_2 -Ar plasma cases. Second, the deviation between the calculated and measured ArH^+ and Ar^+ densities. The experiment shows that n_{ArH^+} is clearly higher than n_{Ar^+} , i.e., by a factor of 4.2 for $f_{\text{Ar}} = 12.6\%$ and by a factor of 1.8 for $f_{\text{Ar}} = 72.3\%$. In contrast, the model predicts roughly the same density for ArH^+ and Ar^+ in the considered Ar fraction range.

The experimentally determined model input parameters have the following influence on the model results: Variations in β_{H} , n_e , and T_e have no or only a moderate influence on the normalized ion densities as shown in Sec. IV D. On the other hand, l_{el} and T_g have a considerable influence on the normalized ion densities. It was shown that an increase of l_{el} or a decrease of T_g lowers the calculated primary ion densities (n_{Ar^+} and $n_{\text{H}_2^+}$) and increases the calculated secondary ion densities (n_{ArH^+} and $n_{\text{H}_3^+}$). Such a change of these input parameters would slightly enhance the agreement between modeled and measured ion densities.

But the model results are also influenced by the rate coefficients. As mentioned in Sec. III E 2, the value of $K_{2.5}$ differs between our study and that of Hjartarson *et al.*

($K_{2.5}^{\text{Hjartarson}}/K_{2.5}^{\text{thiswork}} = 0.027$). However, as shown in Sec. IV A (see Figs. 3(a) and 3(f)), reaction 2.5 has only a small contribution to the total reaction rates of H_3^+ and ArH^+ . Therefore, a lower value for $K_{2.5}$ would only result in a slight modification in our modeled ion densities. Setting this rate coefficient to $K_{2.5}^{\text{Hjartarson}} = 1.0 \times 10^{-17} \text{ m}^3 \text{ s}^{-1}$ would result in a slight increase of $n_{\text{H}_3^+}$ by a factor of about 1.3 and a slight decrease of n_{ArH^+} by a factor of about 1.2. $K_{2.7}$ also differs between our study and that of Hjartarson *et al.* ($K_{2.7}^{\text{Hjartarson}}/K_{2.7}^{\text{thiswork}} = 12$). As shown in Sec. IV A, reaction 2.7 has a negligible contribution to the total reaction rates of H_2^+ and Ar^+ . An increase of $K_{2.7}$ by a factor of 12 would change the resulting ion densities only insignificantly except the H_2^+ density at high $f_{\text{Ar}} \approx 90\%$ which would increase by a factor of about 2. That means that neither a decrease of $K_{2.5}$ nor an increase of $K_{2.7}$ would significantly improve the agreement between model and experimental results.

Further tests have shown that a variation of $K_{2.2}$ (reaction 2.2: $\text{ArH}^+ + \text{H}_2 \rightarrow \text{H}_3^+ + \text{Ar}$) can change the model result considerably. If $K_{2.2}$ is set to 0, the transformation of ArH^+ to H_3^+ is stopped. This results in a higher ArH^+ and a lower H_3^+ density. Because the wall loss coefficient of ArH^+ is lower than that of H_3^+ , this leads to a better confinement and to a higher ArH^+ density. And as a consequence, the plasma density increases. To compensate this, increase in plasma density, T_e^c has to be lowered to fit the quasi-neutrality. Due to this decrease of T_e^c , the ion densities of the primary ions would also change. With $K_{2.2} = 0$, the calculated n_{ArH^+} and n_{Ar^+} dependence on f_{Ar} would agree with the measured values shown in Fig. 7 within the error bars. The calculated $n_{\text{H}_3^+}$ and n_{H^+} densities would also be very close to the measured values. Only the calculated $n_{\text{H}_2^+}$ would remain a factor of about 5 above the measured values indicating the need for a more complex change of the used rate coefficients to fit the experimental ion densities well. Nevertheless, due to the found improvement of the agreement of 5 output values (n_{ArH^+} , n_{Ar^+} , $n_{\text{H}_3^+}$, n_{H^+} , and T_e^c) by only varying the rate coefficient $K_{2.2}$, the reliability of the used value for $K_{2.2}$ has to be questioned.

Up to this point, we concentrated our considerations on the determination of the ion densities in the plasma center. But as mentioned in the introduction, such H_2 -Ar plasmas are frequently used in surface engineering applications. From such an application-oriented perspective, the fluxes arriving at the surface are much more relevant than the species densities. In the following, we will, therefore, calculate the ion fluxes arriving at the surface for a selected plasma condition to highlight the difference between ion densities and ion fluxes. The ion fluxes j_i for the ion species i are calculated by¹⁶

$$j_i = n_i(x_0) \times v_{B,i}, \quad (18)$$

where $v_{B,i}$ is the Bohm velocity (see Sec. III F 1) and $n_i(x_0) = h_l \times n_i$ is the ion density at the sheath edge with h_l defined in Eq. (10). In the following, the ion densities are compared with the corresponding ion fluxes for the case of $f_{\text{Ar}} = 48\%$. For this case, the calculated ion densities of ArH^+ and Ar^+ are by a factor of about two higher than the H_3^+ density (see

Fig. 7). Using Eq. (18) with the calculated ion density values of Fig. 7, the corresponding ion fluxes are $j_{H_3^+} = 2.2 \times 10^{19} \text{ m}^{-2}\text{s}^{-1}$, $j_{ArH^+} = 1.4 \times 10^{19} \text{ m}^{-2}\text{s}^{-1}$, and $j_{Ar^+} = 1.3 \times 10^{19} \text{ m}^{-2}\text{s}^{-1}$. In contrast to the ion densities which are dominated by the Ar-carrying ions, the H_3^+ ion has the largest share of the ion flux. $j_{H_3^+}$ is by a factor of about 1.6 higher than the fluxes of ArH^+ and Ar^+ . This change of the relative contribution of H_3^+ compared with ArH^+ and Ar^+ , if ion fluxes to the surface are considered instead of ion densities in the bulk, is caused by the proportionality $j_i \propto M_i^{-0.5}$. This results in a much higher flux of ions with lower masses compared with the heavier ions. It is further interesting to note that for the considered plasma condition, the flux of atomic H $j_H = n_H v_H / 4$ (see Ref. 24) to the electrode surface is $j_H = 3.4 \times 10^{21} \text{ m}^{-2}\text{s}^{-1}$. This is a factor of 62 higher than the total ion flux $j_{tot} = \sum_i j_i = 5.5 \times 10^{19} \text{ m}^{-2}\text{s}^{-1}$.

VI. SUMMARY

We developed a rate equation model to describe our experimental results of Ref. 16. The model calculates the ion densities n_i , the wall loss probability of atomic hydrogen β_H , and the electron temperature T_e in H_2 -Ar plasmas with different mixing ratios. Input parameters for the model are the required collision rate coefficients. The remaining input parameters are experimentally obtained quantities, namely the electron density n_e , the gas temperature T_g , the total pressure p , the radical density n_H , and the Ar fraction f_{Ar} .

The primary ions H_2^+ and Ar^+ which are produced by ionization of the background gas by electron collisions are effectively converted into H_3^+ and ArH^+ . The Ar-containing ions (Ar^+ and ArH^+) constitute a much higher plasma density than the ions containing only H (H^+ , H_2^+ , H_3^+). This is dominantly due to the much higher loss of H_x^+ ions to the walls due to their lower mass. The H^+/H_2^+ density ratio is closely related to the H/ H_2 density ratio. Because the latter is low, also the H^+/H_2^+ density ratio is low.

Our model describes the measured ion densities of Ref. 16 reasonably well. The main features, i.e., the qualitative abundance of the ion species, the ion density dependence on the Ar fraction, and the electron temperature as function of f_{Ar} , are well reproduced by the model. But some quantitative deviations between model and experiment remain. The two main deviations were discussed; First, the deviations of the calculated and measured H_3^+ and H_2^+ densities and second, the deviation between the calculated and measured ArH^+ and Ar^+ densities. A variation in β_H , n_e , and T_e had no or only a moderate influence on the normalized ion densities. A change of l_{el} and T_g would slightly enhance the agreement between modeled and measured ion densities. The influence of the rate coefficients on the model results was also studied. Neither a decrease of $K_{2,5}$ (rate coefficient of the reaction $H_3^+ + Ar \rightarrow ArH^+ + H_2$) nor an increase of $K_{2,7}$ (rate coefficient of the reaction $Ar^+ + H_2 \rightarrow H_2^+ + Ar$) would significantly improve the agreement between model and experimental results. Only a variation of the rate coefficient $K_{2,2}$ (rate coefficient of the reaction $ArH^+ + H_2 \rightarrow H_3^+ + Ar$) improved the agreement in 5 output values (n_{ArH^+} , n_{Ar^+} , $n_{H_3^+}$, n_{H^+} , and T_e), which gives rise to question the reliability of the used value.

In our model, T_e was fitted to fulfill the quasi-neutrality condition. The modeled T_e shows the same trend as the measured T_e but systematically overestimates the measured values. The calculated atomic hydrogen density n_H^c was fitted to the measured atomic hydrogen density n_H^m through a variation of β_H . The such obtained surface loss probability of atomic hydrogen on stainless steel, β_H , is 0.24 for an assumed H atom temperature of 6000 K.

ACKNOWLEDGMENTS

We gratefully acknowledge help from U. von Toussaint who supported the authors in questions concerning KPP and the error determination of the surface loss probability.

- ¹A. Efremov, N. Min, J. Jeong, Y. Kim, and K. Kwon, "Etching characteristics of Pb(Zr,Ti)O₃, Pt, SiO₂, and Si₃N₄ in an inductively coupled HBr/Ar plasma," *Plasma Sources Sci. Technol.* **19**, 045020 (2010).
- ²S. Yoon, K. Tan, Rusli, and J. Ahn, "Modeling and analysis of hydrogen-methane plasma in electron cyclotron resonance chemical vapor deposition of diamond-like carbon," *J. Appl. Phys.* **91**, 40–47 (2002).
- ³I. B. Denysenko, S. Xu, J. D. Long, R. P. Rutkevych, N. A. Azarenkov, and K. Ostrikov, "Inductively coupled Ar/CH₄/H₂ plasmas for low-temperature deposition of ordered carbon nanostructures," *J. Appl. Phys.* **95**, 2713 (2004).
- ⁴J. Zhou, I. T. Martin, R. Ayers, E. Adams, D. Liu, and E. R. Fisher, "Investigation of inductively coupled Ar and CH₄/Ar plasmas and the effect of ion energy on DLC film properties," *Plasma Sources Sci. Technol.* **15**, 714–726 (2006).
- ⁵J. S. Kim, S. S. Jang, and W. J. Lee, in *Proc. Advanced Metallization and Interconnect Systems for ULSI Applications in 1995* (Materials Research Society, Pittsburgh, 1996), p. 297.
- ⁶A. Weber, R. Nikulski, C.-P. Klages, M. Gross, R. Charatan, R. Opilan, and W. Brown, "Aspects of TiN and Ti deposition in an ECR plasma enhanced CVD process," *Appl. Surf. Sci.* **91**, 314–320 (1995).
- ⁷M. S. Ameen, J. T. Hillman, J. Faguet, R. F. Foster, C. Arena, and F. Martin, in *Proceedings of the Advanced Metallization for ULSI Applications in 1994*, edited by R. Blumenthal (Materials Research Society, Pittsburgh, 1995), p. 269.
- ⁸R. A. Ditzio, G. Liu, S. J. Fonash, B.-C. Hsieh, and D. W. Greve, "Short time electron cyclotron resonance hydrogenation of polycrystalline silicon thin-film transistor structures," *Appl. Phys. Lett.* **56**, 1140–1142 (1990).
- ⁹E. S. Cielaszyk, K. H. R. Kirmse, R. A. Stewart, and A. E. Wendt, "Mechanisms for polycrystalline silicon defect passivation by hydrogenation in an electron cyclotron resonance plasma," *Appl. Phys. Lett.* **67**, 3099–3101 (1995).
- ¹⁰R. A. Gottscho, B. L. Preppernau, S. J. Pearton, A. B. Emerson, and K. P. Giapis, "Real-time monitoring of low temperature hydrogen plasma passivation of GaAs," *J. Appl. Phys.* **68**, 440–445 (1990).
- ¹¹J. D. Bernstein, S. Qing, C. Chan, and T.-J. King, "High dose-rate hydrogen passivation of polycrystalline silicon CMOS TFTs by plasma ion implantation," *IEEE Trans. Electron Devices* **43**, 1876–1882 (1996).
- ¹²C.-F. Yeh, T.-J. Chen, C. Liu, J. Gudmundsson, and M. Lieberman, "Hydrogenation of polysilicon thin-film transistor in a planar inductive H₂/Ar discharge," *IEEE Electron Device Lett.* **20**, 223–225 (1999).
- ¹³N. Fox-Lyon, G. S. Oehrlein, N. Ning, and D. B. Graves, "Hydrogenation and surface density changes in hydrocarbon films during erosion using Ar/H₂ plasmas," *J. Appl. Phys.* **110**, 104314 (2011).
- ¹⁴C. Hopf, A. von Keudell, and W. Jacob, "Chemical sputtering of hydrocarbon films," *J. Appl. Phys.* **94**, 2373–2380 (2003).
- ¹⁵V. S. Voitsenya, D. I. Naidenkov, Y. Kubota, S. Masuzaki, A. Sagara, and K. Yamazaki, "On the possibility to increase efficiency of conditioning of vacuum surfaces by using a discharge in a hydrogen-noble gas mixture," *Natl. Inst. Fusion Sci.* **799**, 1 (2004).
- ¹⁶M. Sode, T. Schwarz-Selinger, and W. Jacob, "Quantitative determination of mass-resolved ion densities in H₂-Ar inductively coupled radio frequency plasmas," *J. Appl. Phys.* **113**, 093304 (2013).
- ¹⁷T. Kimura and H. Kasugai, "Properties of inductively coupled rf Ar/H₂ plasmas: Experiment and global model," *J. Appl. Phys.* **107**, 083308 (2010).

- ¹⁸A. T. Hjartarson, E. G. Thorsteinsson, and J. T. Gudmundsson, "Low pressure hydrogen discharges diluted with argon explored using a global model," *Plasma Sources Sci. Technol.* **19**, 065008 (2010).
- ¹⁹J. T. Gudmundsson, "Experimental studies of H₂/Ar plasma in a planar inductive discharge," *Plasma Sources Sci. Technol.* **7**, 330–336 (1998).
- ²⁰J. T. Gudmundsson, "Ion energy distribution in H₂/Ar plasma in a planar inductive discharge," *Plasma Sources Sci. Technol.* **8**, 58–64 (1999).
- ²¹I. Méndez, I. Tanarro, and V. J. Herrero, "On the ionic chemistry in DC cold plasmas of H₂ with Ar," *Phys. Chem. Chem. Phys.* **12**, 4239–4245 (2010).
- ²²I. Tanarro and V. J. Herrero, "Large effects of small pressure changes in the kinetics of low pressure glow discharges," *Plasma Sources Sci. Technol.* **20**, 024006 (2011).
- ²³V. A. Kadetov, "Diagnostics and modeling of an inductively coupled radio frequency discharge in hydrogen," Ph.D. dissertation (Ruhr Universität Bochum, 2004).
- ²⁴M. A. Lieberman and A. J. Lichtenberg, *Principles of Plasma Discharges and Materials Processing* (John Wiley and Sons, Inc., Hoboken, New Jersey, 2005).
- ²⁵C. Lee, D. B. Graves, M. A. Lieberman, and D. W. Hess, "Global model of plasma chemistry in a high density oxygen discharge," *J. Electrochem. Soc.* **141**, 1546 (1994).
- ²⁶K. Tao, D. Mao, and J. Hopwood, "Ionized physical vapor deposition of titanium nitride: A global plasma model," *J. Appl. Phys.* **91**, 4040–4048 (2002).
- ²⁷A. Sandu and R. Sanders, KPP—The kinetic preprocessor, Version 2.2.1 (2006), <http://people.cs.vt.edu/asandu/Software/Kpp/>.
- ²⁸V. Damian, A. Sandu, M. Damian, F. Potra, and G. R. Carmichael, "The kinetic preprocessor KPP—a software environment for solving chemical kinetics," *Comput. Chem. Eng.* **26**, 1567–1579 (2002).
- ²⁹J.-S. Yoon, M.-Y. Song, J.-M. Han, S. H. Hwang, W.-S. Chang, B. Lee, and Y. Itikawa, "Cross sections for electron collisions with hydrogen molecules," *J. Phys. Chem. Ref. Data* **37**, 913–931 (2008).
- ³⁰M. B. Shah, D. S. Elliott, and H. B. Gilbody, "Pulsed crossed-beam study of the ionisation of atomic hydrogen by electron impact," *J. Phys. B* **20**, 3501–3514 (1987).
- ³¹R. C. Wetzel, F. A. Baiocchi, T. R. Hayes, and R. S. Freund, "Absolute cross sections for electron-impact ionization of the rare-gas atoms by the fast-neutral-beam method," *Phys. Rev. A* **35**, 559–577 (1987).
- ³²A. Florescu-Mitchell and J. Mitchell, "Dissociative recombination," *Phys. Rep.* **430**, 277–374 (2006).
- ³³H. C. Straub, P. Renault, B. G. Lindsay, K. A. Smith, and R. F. Stebbings, "Absolute partial and total cross sections for electron-impact ionization of argon from threshold to 1000 eV," *Phys. Rev. A* **52**, 1115–1124 (1995).
- ³⁴R. K. Janev, W. D. Langer, K. Evans, and D. E. Post, *Elementary Processes in Hydrogen-Helium Plasmas* (Springer-Verlag, Berlin, 1987).
- ³⁵V. K. Anicich, "Evaluated bimolecular ion-molecule gas phase kinetics of positive ions for use in modelling planetary atmospheres, cometary comae, and interstellar clouds," *J. Phys. Chem. Ref. Data* **22**, 1469–1569 (1993).
- ³⁶A. Bogaerts and R. Gijbels, "Hybrid Monte Carlo—fluid modeling network for an argon/hydrogen direct current glow discharge," *Spectrochim. Acta Part B* **57**, 1071–1099 (2002).
- ³⁷P. B. Armentrout, "Fundamentals of ion-molecule chemistry," *J. Anal. At. Spectrom.* **19**, 571–580 (2004).
- ³⁸M. Osiac, T. Schwarz-Selinger, D. O'Connell, B. Heil, Z. L. Petrovic, M. M. Turner, T. Gans, and U. Czarnetzki, "Plasma boundary sheath in the afterglow of a pulsed inductively coupled RF plasma," *Plasma Sources Sci. Technol.* **16**, 355–363 (2007).
- ³⁹V. A. Godyak, *Soviet Radio Frequency Discharge Research* (Delphic Associates, Falls Church, VA, 1986).
- ⁴⁰P. J. Chantry, "A simple formula for diffusion calculations involving wall reflection and low density," *J. Appl. Phys.* **62**, 1141–1148 (1987).
- ⁴¹M. A. Biondi and L. M. Chanin, "Blanc's law—ion mobilities in helium-neon mixtures," *Phys. Rev.* **122**, 843–847 (1961).
- ⁴²E. Tatarova, F. M. Dias, C. M. Ferreira, and N. Puac, "Spectroscopic determination of H, He, and H₂ temperatures in a large-scale microwave plasma source," *J. Appl. Phys.* **101**, 063306 (2007).
- ⁴³U. Cvelbar, M. Mozetič, I. Poberaj, D. Babič, and A. Ricard, "Characterization of hydrogen plasma with a fiber optics catalytic probe," *Thin Solid Films* **475**, 12–16 (2005).
- ⁴⁴J. Jolly and J.-P. Booth, "Atomic hydrogen densities in capacitively coupled very high-frequency plasmas in H₂: Effect of excitation frequency," *J. Appl. Phys.* **97**, 103305 (2005).
- ⁴⁵P. Kae-Nune, J. Perrin, J. Jolly, and J. Guillon, "Surface recombination probabilities of H on stainless steel, a-Si:H and oxidized silicon determined by threshold ionization mass spectrometry in H₂ RF discharges," *Surf. Sci. Lett.* **360**, L495 (1996).
- ⁴⁶W. Press, S. Teukolsky, W. Vetterlin, and B. Flannery, *Numerical Recipes*, 3rd ed. (Cambridge University Press, Cambridge, 2007).
- ⁴⁷M. Gerl, "Modellierung von Teilchendichten in Stickstoff-Niedertemperaturplasmen," Bachelors thesis (Technische Universität München, 2011) (in German).
- ⁴⁸I. Denysenko, I. Stefanovic, B. Sikimic, J. Winter, N. A. Azarenkov, and N. Sadeghi, "A global model for the afterglow of pure argon and of argon with negatively charged dust particles," *J. Phys. D* **44**, 205204 (2011).
- ⁴⁹D. P. Lymberopoulos and D. J. Economou, "Fluid simulations of glow discharges: Effect of metastable atoms in argon," *J. Appl. Phys.* **73**, 3668–3679 (1993).